Loss of eIF4E phosphorylation engenders depression-like behaviors via selective mRNA translation

JNeurosci
THE JOURNAL OF NEUROSCIENCE

Research Articles: Neurobiology of Disease

Loss of eIF4E phosphorylation engenders depression-like behaviors via selective mRNA translation

Inês Silva Amorim[1,2], Sonal Kedia[1,2], Stella Kouloulia[1,2], Konstanze Simbriger[1,2], Ilse Gantois[3], Seyed Mehdi Jafarnejad[3], Yupeng Li[1,2], Agniete Kampaite[1,2], Tine Pooters[1], Nicola Romanò[1] and Christos G. Gkogkas[1,2,4]

[1]*Centre for Discovery Brain Sciences, EH8 9XD, Edinburgh, Scotland, UK*

[2]*The Patrick Wild Centre, EH8 9XD, Edinburgh, Scotland, UK*

[3]*Goodman Cancer Research Centre and Biochemistry Department, McGill University, H3A 1A3, Montréal, QC, Canada*

[4]*Simons Initiative for the Developing Brain, EH8 9XD, Edinburgh, Scotland, UK*

DOI: 10.1523/JNEUROSCI.2673-17.2018

Received: 16 September 2017

Revised: 3 December 2017

Accepted: 8 January 2018

Published: 24 January 2018

Author contributions: I.S.A., S. Kedia, S. Kouloulia, S.M.J., N.R., and C.G.G. designed research; I.S.A., S. Kedia, S. Kouloulia, K.S., I.G., S.M.J., Y.L., A.K., N.R., and C.G.G. performed research; I.S.A., S. Kedia, S. Kouloulia, K.S., I.G., S.M.J., A.K., T.P., and C.G.G. analyzed data; N.R. and C.G.G. contributed unpublished reagents/analytic tools; C.G.G. wrote the paper.

Conflict of Interest: The authors declare no competing financial interests.

This work was supported by grants to CGG: Sir Henry Dale Fellowship from the Wellcome Trust and Royal Society (107687/Z/15/Z), a NARSAD Young Investigator grant from the Brain & Behavior Research Foundation, the RS Macdonald Charitable Trust and the Patrick Wild Centre. We thank M. Laidlaw, C. Wollaston, R. Loureiro and T. Amvrosiadis for technical assistance.

Corresponding author: Christos G. Gkogkas, Centre for Discovery Brain Sciences, The Patrick Wild Centre and Simons Initiative for the Developing Brain, Hugh Robson Building, George Square, EH89XD, Edinburgh, UK, christos.gkogkas@ed.ac.uk

Cite as: J. Neurosci ; 10.1523/JNEUROSCI.2673-17.2018

Loss of eIF4E phosphorylation engenders depression-like behaviors via selective mRNA translation

Abbreviated title: The role of eIF4E phosphorylation in depression

Inês Silva Amorim[1,2*], Sonal Kedia[1,2*], Stella Kouloulia[1,2*], Konstanze Simbriger[1,2*], Ilse Gantois[3], Seyed Mehdi Jafarnejad[3], Yupeng Li[1,2], Agniete Kampaite[1,2], Tine Pooters[1], Nicola Romanò[1], and Christos G. Gkogkas[1,2,4#].

[1]Centre for Discovery Brain Sciences, EH8 9XD, Edinburgh, Scotland, UK
[2]The Patrick Wild Centre, EH8 9XD, Edinburgh, Scotland, UK
[3]Goodman Cancer Research Centre and Biochemistry Department, McGill University, H3A 1A3, Montréal, QC, Canada
[4]Simons Initiative for the Developing Brain, EH8 9XD, Edinburgh, Scotland, UK

[*]these authors contributed equally

[#]**Corresponding author**: Christos G. Gkogkas, Centre for Discovery Brain Sciences, The Patrick Wild Centre and Simons Initiative for the Developing Brain, Hugh Robson Building, George Square, EH89XD, Edinburgh, UK, christos.gkogkas@ed.ac.uk

Pages: (32)

Figures (7), Tables (2), Multimedia (0) and 3D models (0), Extended Figure (1)

Number of words for Abstract (217), Introduction (625), and Discussion (1417)

Conflict of Interest: None declared

Acknowledgements: This work was supported by grants to CGG: Sir Henry Dale Fellowship from the Wellcome Trust and Royal Society (107687/Z/15/Z), a NARSAD Young Investigator grant from the Brain & Behavior Research Foundation, the RS Macdonald Charitable Trust and the Patrick Wild Centre. We thank M. Laidlaw, C. Wollaston, R. Loureiro and T. Amvrosiadis for technical assistance.

Abstract (217 words**)**

The MAPK/ERK (Mitogen Activated Protein Kinases/Extracellular signal-Regulated Kinases) pathway is a cardinal regulator of synaptic plasticity, learning and memory in the hippocampus. One of major endpoints of this signaling cascade is the 5′ mRNA cap-binding protein eIF4E (eukaryotic Initiation Factor 4E), which is phosphorylated on Ser 209 by MNK (MAPK-interacting protein kinases) and controls mRNA translation. The precise role of phospho-eIF4E in the brain is yet to be determined. Herein, we demonstrate that ablation of eIF4E phosphorylation in male mice (4Eki mice) does not impair long-term spatial or contextual fear memory, or the late phase of long-term potentiation (L-LTP). Using unbiased translational profiling in mouse brain, we show that phospho-eIF4E differentially regulates the translation of a subset of mRNAs linked to inflammation, the extracellular matrix (ECM), pituitary hormones and the serotonin pathway. Consequently, 4Eki male mice display exaggerated inflammatory responses and reduced levels of serotonin, concomitant with depression and anxiety-like behaviors. Remarkably, eIF4E phosphorylation is required for the chronic antidepressant action of the selective serotonin reuptake inhibitor (SSRI) fluoxetine. Finally, we propose a novel phospho-eIF4E-dependent translational control mechanism in the brain, via the GAIT complex (Gamma interferon Activated Inhibitor of Translation). In summary, our work proposes a novel translational control mechanism involved in the regulation of inflammation and depression, which could be exploited to design novel therapeutics.

Significance Statement (122)

We demonstrate that downstream of the Mitogen Activated Protein Kinase (MAPK) pathway, eukaryotic Initiation Factor 4E (eIF4E) Ser209 phosphorylation is not required for classical forms of hippocampal long-term potentiation and memory. We reveal a novel role for eIF4E phosphorylation in inflammatory responses and depression-like behaviors. eIF4E phosphorylation is required for the chronic action of antidepressants such as fluoxetine in mice. These phenotypes are accompanied by selective translation of extracellular matrix, pituitary hormones and serotonin pathway genes, in eIF4E phospho-mutant mice. We also describe a previously unidentified translational control mechanism in the brain, whereby eIF4E phosphorylation is required for inhibiting the translation of Gamma interferon Activated Inhibitor of Translation (GAIT) element-containing mRNAs. These findings can be used to design novel therapeutics for depression.

Introduction (625 words)

MAPK/ERK is a conserved signaling pathway, which in response to a plethora of intracellular and extracellular signals such as cytokines, mitogens, growth factors, hormones and neurotransmitters, elicits changes in cellular gene-expression programs (Kelleher et al., 2004; Thomas and Huganir, 2004). In the brain, activation of MAPK/ERK in response to excitatory glutamatergic signaling, has been linked to regulation of synaptic plasticity, learning and memory (English and Sweatt, 1997; Zhu et al., 2002; Kelleher et al., 2004; Thomas and Huganir, 2004). Indeed, long-term potentiation of excitatory synaptic transmission, mainly in the mammalian hippocampus, requires MAPK/ERK activity (Kanterewicz et al., 2000; Kelleher et al., 2004). Accordingly, MAPK/ERK inhibition impairs learning and hippocampal spatial memory (Atkins et al., 1998) and fear conditioning in rodents (Schafe et al., 2000).

Downstream of MAPK/ERK, the MNK1/2 kinases regulate mRNA translation (Joshi and Platanias, 2014) mainly by phosphorylating eIF4E on Ser209 (Flynn and Proud, 1995; Joshi et al., 1995). eIF4E binds to the mRNA 5′ cap, and together with eIF4G (scaffolding protein) and eIF4A (mRNA helicase) form the eIF4F complex, promoting translation initiation (Hinnebusch et al., 2016). eIF4E stimulates the translation of a subset of mRNAs ('eIF4E-sensitive'), without upregulating global protein synthesis (Hinnebusch et al., 2016). eIF4E, apart from its primary cap-binding function, also promotes mRNA restructuring and initiation by stimulating eIF4A helicase activity (Feoktistova et al., 2013). Thus, eIF4E-sensitive mRNAs contain long and highly structured 5′UTRs (such as proto-oncogenes and growth factors), which require elevated helicase activity for their translation (Sonenberg and Hinnebusch, 2009).

Most of the current literature posits that eIF4E phosphorylation promotes mRNA translation (Pyronnet et al., 1999; Lachance et al., 2002; Panja et al., 2014; Bramham et al., 2016). It was also suggested that eIF4E phosphorylation is not required for translation (McKendrick et al., 2001), or that it decreases cap-dependent translation (Knauf et al., 2001). Several studies identified phospho-eIF4E-sensitive mRNAs in cancer models (Furic et al., 2010; Konicek et al., 2011; Robichaud et al., 2015), however in brain, only a small subset was revealed. In the hippocampus, phospho-eIF4E regulates the translation of *Mmp9* (Gkogkas et al., 2014; Gantois et al., 2017), while in the suprachiasmatic nucleus phospho-eIF4E controls the translation of *Per1/2* mRNAs (Cao et al., 2015). Interestingly, phospho-eIF4E is a master

regulator of type I interferon production, and thus of the antiviral response, by controlling the translation of *NFKBIA* mRNA (coding for IκBα protein; nuclear factor of kappa light polypeptide gene enhancer in B-cells inhibitor, alpha)(Herdy et al., 2012). Ablation of phospho-eIF4E downregulates IκBα and activates the transcription factor NF-κB, which regulates cytokine production and antiviral responses (Herdy et al., 2012). Whereas phospho-eIF4E has been implicated in the regulation of some brain functions (Gkogkas et al., 2014; Cao et al., 2015), its precise role in the brain, is yet to be elucidated. Little is also known about the subset of phospho-eIF4E-dependent mRNAs or about the regulatory mechanisms governing their translation in the brain.

Herein, we show that in mice lacking eIF4E phosphorylation (4Eki) hippocampal long-term spatial and fear memory formation, and L-LTP are intact. Using unbiased ribosome profiling in 4Eki brains, we identified reduced translation of mRNAs coding for extracellular matrix proteins and pituitary hormones and, unexpectedly, increased translation of serotonin pathway and ribosomal protein mRNAs. This altered translational landscape in 4Eki brain is accompanied by exaggerated inflammatory responses and reduced brain serotonin levels. Subsequently, we show that 4Eki mice display depression-like behaviors, which are resistant to chronic treatment with the selective serotonin reuptake inhibitor (SSRI) antidepressant fluoxetine. We demonstrate a potential mechanism for phospho-eIF4E translational control in the brain, which is mediated by altered GAIT-dependent translation and reduced binding of eIF4A1 to the 5´mRNA cap. Together, these data establish a previously unidentified role for eIF4E phosphorylation in depression due to selective translation of a subset of mRNAs.

Materials & Methods

Transgenic Mice

All procedures were in accordance with UK Home Office and Canadian Council on Animal Care regulations and were approved by the University of Edinburgh and McGill University. *eIF4E*^{Ser209Ala} mice were previously described (Gkogkas et al., 2014) and were maintained on the C57Bl/6J background (backcrossed for more than 10 generations). For most experiments, male mice aged 8-12 weeks were used (for slice electrophysiology 6-8-week-old males were used). Food and water were provided *ad libitum*, and mice were kept on a 12h light/dark cycle. Pups were kept with their dams until weaning at postnatal day 21. After weaning, mice

were group housed (maximum of 4 per cage) by sex. Cages were maintained in ventilated racks in temperature (20-21^{o}C) and humidity (~55%) controlled rooms, on a 12-hour circadian cycle (7am-7pm light period). For all behavioral testing, mice were handled/habituated for 3-4 consecutive days prior to experimental testing. Fluoxetine hydrochloride (Sigma) or vehicle (saline) were injected at 10 mg/kg intraperitoneally for 21 days. Lipopolysaccharide (LPS, strain O111:B4; Sigma) or vehicle (saline), were injected at 5 mg/kg intraperitoneally and brains were collected 4h later.

Morris Water Maze (MWM)

Mice were handled for 3 days before the experiment. Training in the pool (100 cm diameter and 10cm diameter platform; water temperature was 24^{o}C) consisted of three trials per day (20 min inter-trial interval), where each mouse swam until it reached the hidden platform. Animals that did not find the platform after 60 s were gently guided to it and would remain there for 10 s prior to returning them to the cage. For the probe test, the platform was removed and animals could swim for 60 s. The swimming trajectory and velocity were monitored with a video tracking system (HVS Image).

Contextual Fear Conditioning (CFC)

Mice were handled for 3–4 days before the start of the experiment and then conditioned in the chamber: 2 min acclimatization to the context, followed by the unconditioned stimulus (US); one foot shock (0.5 mA, 4 s) followed by a 30 s interval, terminating with another identical foot shock. The mice remained in the chamber for an additional 1 min after the end of the last US, after which they were returned to their home cages. Contextual fear memory was assayed 24 h after training by re-exposing the animals to the conditioning context for a 5-min period. During this period, the incidence of freezing (immobile except for respiration) was recorded (FreezeFrame, Coulbourn Instruments). Freezing behavior was analyzed by assigning at 5 s intervals as either freezing or not freezing. Data are expressed as the percentage of 5 s intervals scored as “freezing”.

Forced Swim Test (FST)

Transparent glass cylinders (50 cm height x 20 cm diameter) were filled with tap water maintained at 25 °C. The water depth was adjusted according to the size of the mouse, so that it could not touch the bottom of the container with its hind legs. Animals were tested for 6 min, while only the last 4 min were scored for immobility using a manual timer.

Tail Suspension Test (TST)

Each mouse was suspended within its own three-walled (white) rectangular compartment (55cm height X 15cm width X 11.5 cm depth) in the middle of an aluminum suspension bar using adhesive tape. The width and depth are sufficiently sized so that the mouse cannot touch the walls. The duration of the test is 5 min and immobility was manually scored with a timer.

Novelty Suppressed Feeding (NSF)

Mice were handled for 3 days and following 24h food deprivation were placed in a 40 x 40 cm^2 open field arena for 5 min. Weight loss was <7% and no difference was seen between genotypes. At the centre of the arena 2 food pellets were fixed on a Whatman paper covered circular platform (replaced between subjects) glued on a 10m petri-dish, to stop mice from removing the pellets. Animals that did not consume the pellets within the testing period were assigned to a latency of 300s. The latency to grab food with both limbs and commence eating was measured with a stop watch and animals were weighed prior to the start of the experiment.

Open Field Test (OF)

Mice were handled for 3-4 days and then allowed to freely explore a 40 x 40 cm^2 open field arena for 10 min. A 20 x 20 cm center region was designated as the center square. Time in the center square and outside, as well as total distance travelled were recorded.

Elevated Plus Maze (EPM)

Mice were handled for 3-4 days and then allowed to freely explore an elevated plus maze (50cm from ground), with open (2) and closed (2) arms: 50cm length x 10cm width and 40cm height for the walls of closed arms. Time spent in the closed and open arms over a period of 5 min was manually recorded using a handheld timer.

Extracellular Field Recordings

Transverse hippocampal slices (400 μm) were prepared from WT or 4Eki males (6–8 weeks old). Slices were then allowed to recover submerged for at least 1 h at 32°C in oxygenated artificial cerebrospinal fluid (ACSF) containing 124 mM NaCl, 2.5 mM KCl, 1.25 mM NaH_2PO_4, 25 mM $NaHCO_3$, 20 mM glucose, 1 mM $MgCl_2$, and 2 mM $CaCl_2$ before

transferring to a recording chamber at 29°C–31°C which was continuously perfused with ACSF. Field Excitatory Postsynaptic Potentials (fEPSPs) were recorded in CA1 stratum radiatum with glass electrodes (2–3 MΩ) filled with ACSF. Schaffer collateral fEPSPs were evoked with a twisted bipolar stimulating electrode placed in stratum radiatum proximal to CA3 region. All signals collected were analyzed using WinLTP program. Test pulses were adjusted to obtain 40%–50% maximal fEPSP, delivered every 30 s and averaged over 1 min. Basal responses were measured 60 min prior to the LTP stimulus. For the induction of L-LTP, four 1 s trains of 100 Hz high frequency stimulation were delivered with an inter-train interval of 5 min. The initial slopes of the fEPSPs were measured and values were normalized to the averaged baseline slope value for each slice. Percentage of potentiation was calculated as the difference between averaged values for a 10-min period before the tetanus and the last 10 min of recording.

Immunoblotting

Dissected brain tissue was homogenized in buffer B (50 mM MOPS/KOH pH 7.4, 100 mM NaCl, 50 mM NaF, 2 mM EDTA, 2 mM EGTA, 1% NP-40, 7 mM β-mercaptoethanol) supplemented with protease and phosphatase inhibitors (Roche). Samples were incubated on ice for 15 min, with occasional vortexing, and cleared by centrifugation for 20 min at 16,000*g* at 4°C. The supernatant was used for western blotting after the protein concentration of each sample was determined by measuring A280 Absorbance on a NanoDrop (ThermoFisher Scientific). 50 µg of protein per lane were prepared in SDS Sample Buffer (50mM Tris pH 6.8, 100 mM DTT, 2% SDS, 10% Glycerol, 0.1% bromophenol blue), heated to 98°C for 5 min and resolved on 10-16% polyacrylamide gels. Proteins were transferred to 0.2 µm nitrocellulose membranes (Bio-Rad), blocked in 5% BSA in TBS-T (10 mM Tris pH 7.6, 150 mM NaCl, 0.1% Tween-20) for 1 h at RT, incubated with primary antibodies overnight at 4°C and with secondary antibodies for 1 h at RT. Primary antibodies were diluted in 1% BSA in TBS-T containing 0.02% Na azide, and between incubations membranes were washed extensively in TBS-T. Blots were imaged using an Odyssey Imaging System (Li-COR Biosciences) at a resolution of 169 µm and quantified using the ImageStudio Software (Li-COR Biosciences). For quantitative Western Blotting, the intensity of each protein band was measured in triplicate to minimize measuring variability. HSC70 or *β*-actin were used as a loading control. Data are shown as arbitrary units (AU) after normalization to control.

Antibodies

The antibodies used for immunoblotting or immunofluorescence are summarized in Table 1.

Immunofluorescence and Confocal Imaging

Mice were anaesthetized and transcardially perfused with 4% paraformaldehyde (PFA; Electron Microscopy Sciences) in PBS. The brain was immediately dissected from the skull, post-fixed in 4% PFA in PBS overnight at 4°C and cryopreserved in a solution of 30% sucrose in PBS for 48 h at 4°C. Each brain was embedded in a mixture (1:1) of OCT:30% sucrose and 30 µm coronal sections were cut on a cryostat (Leica). Sections were stored at 4°C as floating sections in PBS with 0.02% Na azide, until used. Sections were then incubated in blocking solution (5% Normal Goat Serum (NGS; Cell Signaling), 0.3% Triton X-100 (Sigma) in PBS for 1 h at RT, washed briefly in PBS and incubated with primary antibodies overnight at 4°C and with secondary antibodies for 2h at RT. The antibodies were diluted in 2% NGS, 0.1% Triton X-100 in PBS and the sections were washed extensively in PBS between incubations. A nuclear counterstain was applied by incubating the sections for 5 min with DAPI solution (1 µg/mL; ThermoFisher Scientific). Sections were mounted on glass slides using PermaFluor Mounting Media (ThermoFisher Scientific), protected with a glass coverslip and stored at 4°C in the dark. Images were collected on a Zeiss LSM800 confocal microscope.

Quantitative ELISA for Cytokines and Serotonin

Forebrain tissue was homogenized in kit sample buffer (QiaMouse Inflammatory Cytokines, Generon Iba1 or Chemokines Multi-Analyte ELISArray Kit, Qiagen and Serotonin ELISA kit, Enzo Life Sciences) with ~30 strokes in a glass Dounce homogenizer on ice. Lysates were centrifuged at 16,000*g* for 5 min and the supernatant was used for the assay. Detection was carried out as per each kit's guidelines. For both assays 50 µg of total protein was analyzed per sample (measured by Bradford assay, Bio-Rad). Optical density values were converted to pg/mg of total protein using curves of OD versus kit standard cytokine concentrations. In brain tissue, we detected the following cytokines from the kit: IL1B, IL2, IL6, IL10, IFNγ and TNFα and Iba1 and serotonin as mg/pg of tissue.

Ribosome Profiling and Bioinformatics Analysis

Flash frozen forebrain tissue was pulverized using liquid nitrogen, and then lysed in hypotonic buffer; 5 mM Tris-HCl (pH 7.5), 2.5 mM MgCl2, 1.5 mM KCl, 1x protease inhibitor cocktail (EDTA-free), 100µg/ml cycloheximide (Sigma), 2 mM DTT, 200 U/ml RNaseIn), 0.5% (w/v) Triton X-100, and 0.5% (w/v) sodium deoxycholate, to isolate the polysomes with centrifugation (20,000*g*) at 4^{o}C for 5 min. Ribosome profiling was performed as previously described (Ingolia et al., 2012), with minor modifications. Briefly, 500 µg of the lysed RNPs (forebrain tissue) were subjected to ribosome footprinting by RNase I treatment at 4^{o}C for 45 min with gentle mixing. Monosomes were pelleted by ultracentrifugation in a 34% sucrose cushion at 70,000 RPM for 3 h and RNA fragments were extracted twice with acid phenol, once with chloroform, and precipitated with isopropanol in the presence of NaOAc and GlycoBlue. Purified RNA was resolved on a denaturing 15% polyacrylamide urea gel and the section corresponding to 28-32 nucleotides containing the ribosome footprints (RFPs) was excised, eluted, and precipitated by isopropanol. 100 µg of cytoplasmic RNA was used for mRNA-Seq analysis. Poly (A)+ mRNAs were purified using magnetic oligo-dT DynaBeads (Invitrogen) according to the manufacturer's instructions. Purified RNA was eluted from the beads and mixed with an equal volume of 2X alkaline fragmentation solution (2 mM EDTA, 10 mM Na_2CO_3, 90 mM $NaHCO_3$, pH 9.2) and incubated for 20 min at 95^{o}C. Fragmentation reactions were mixed with stop/precipitation solution (300 mM NaOAc pH 5.5 and GlycoBlue), followed by isopropanol precipitation. Fragmented mRNA was size-selected on a denaturing 10% polyacrylamide urea gel and the area corresponding to 35-50 nucleotides was excised, eluted, and precipitated with isopropanol. All samples were analyzed on an Agilent Bioanalyzer High Sensitivity DNA chip to confirm expected size range and quantity and sequenced on an Illumina HiSeq 2500 system. Raw sequencing data were de-multiplexed by the sequencing facility (Genome Quebec). Sequences were analyzed using a custom developed bioinformatics pipeline adapted from (Ingolia et al., 2012). Reads were adapter-trimmed using the FASTX toolkit, contaminant sequences (rRNA, tRNA) removed using bowtie and reads aligned to a reference genome using STAR. Cufflinks was used to quantify reads and calculate Reads Per Kilobase of transcript per Million mapped reads (RPKM) for each transcript. Translational efficiency (TE) for each transcript was calculated by dividing RPKM values of the RPF libraries by RPKM values of the Total RNA libraries. Changes in TE and transcription (mRNA RPKM) values were analyzed for predefined pairwise comparisons between experimental groups, employing methods reviewed in (Quackenbush, 2002). First, averages were calculated for replicate TE/RPKM values of each treatment on a per-gene

basis using the geometric mean. From these averages, two statistics were derived for each gene: 1) Ratio, defined as the quotient of values for alternative treatment (e.g. knock-in) and base level treatment (e.g. wild type); 2) Intensity, defined as the product of the afore-mentioned values. Data were ordered by increasing $\log_{10}$(Intensity). Along this ordered set of values, mean $\log_{10}$ (Intensity) as well as mean and standard deviation of $\log_2$(Ratio) were calculated within a sliding window of 100 genes at steps of 50 genes. Each gene was assigned to the window with a mean $\log_{10}$ (Intensity) closest to the gene's $\log_{10}$(Intensity). A z-score was then calculated for the i^{th} gene using its window's $\log_2$(Ratio) mean and standard deviation:

$$z_i = \frac{log_2(Ratio_i) - \mu^{window}_{log_2(Ratio)}}{\sigma^{window}_{log_2(Ratio)}}$$

A p-value was derived from the z-score of the i^{th} gene by treating the latter as a quantile of the standard normal distribution:

$$p_i = 2 \times (1 - \phi_{(|zi|)})$$

False-discovery rates (FDR) were calculated from p-values derived with the z-score as in (Reiner et al., 2003). Genes with <128 reads were discarded. Raw RNAseq data will be deposited to NCBI Gene Expression Omnibus (GEO).

Principal Components Analysis and Hierarchical Clustering

Principal Component Analysis (PCA) was conducted with R package vegan v2.4.4 (Oksanen et al., 2017). Genes with undefined log2-transformed values (for RPKM = 0 or TE = 0) were excluded from the analysis. $\log_2$-transformed values of the remaining set of genes were standardized on a per-gene basis (scaled to mean = 0 and standard deviation = 1). Euclidean distances of samples (replicates) were calculated from the same standardized log2-transformed gene data used in PCA. Hierarchical Clustering based on the complete-linkage algorithm was performed on the distance matrix with R package stats v3.4.2. Results were visualized as dendrograms below the corresponding PCA plot.

g:profiler Analysis of mRNAs

Functional enrichment analysis was carried using the g:Ghost package of g:profiler to assign Gene Ontology categories to ribosome profiling lists of differentially translated genes (Reimand et al., 2016). Hierarchical filtering was used - best per parent group-strong. The probability threshold for all functional categories was set at 0.05, using correction for multiple testing with the g:SCS algorithm (Reimand et al., 2016).

UTR Sequence Analysis

UTR sequence analysis was carried out using RegRNA (Huang et al., 2006). Motifs in 5′ and 3′ UTR were detected with default parameters. 652 downregulated, 52 upregulated and 325 control mRNA UTRs were obtained from Biomart ENSEMBL (Yates et al., 2016) using the GRCm38.p5 version of the mouse genome. Length in BP and %GC content were calculated using free Python-based scripts (Multifastats; https://github.com/davidrequena/multifastats).

Cap column Pulldown

Forebrain tissue was dissected and lysates were prepared in the same way as for immunoblotting (see above). 500 µg of protein were incubated with 50 µL of m^7GDP agarose (Jena Biosciences), in a total volume of 1 mL Buffer C (50 mM MOPS-KOH pH 7.4, 100 mM NaCl, 50 mM NaF, 0.5 mM EDTA, 0.5 mM EGTA, 7 mM β-mercaptoethanol, 0.5 mM PMSF, 1 mM Na_3VO_4 and 0.1 mM GTP), for 90 min at 4°C with rotation. The beads were washed three times in Buffer C and the cap-bound fraction was eluted in 50 µL of 2X SDS Sample Buffer with boiling at 70^{o}C for 10 min.

Experimental Design and Statistical analysis

Experimenters were blinded to the genotype during testing and scoring. All data are presented as mean ±S.E.M. (error bars) and individual experimental points are depicted in column or bar graphs. Statistical significance was set *a priori* at 0.05 (n.s.: non-significant). Fluoxetine treatment was randomized across cages (not all animals in one cage received the same treatment; vehicle or fluoxetine). No nested data were obtained in this study; we only collected one observation per research object. Details for statistical tests used were provided within figure legends or the relative methods description and summarized in Table 2. Data summaries and statistical analysis were carried out using Graphpad Prism 6 and SPSS v. 21.

Results

Loss of eIF4E phosphorylation does not affect hippocampal learning, memory or late-LTP

eIF4E is highly expressed throughout the hippocampal formation (Fig. 1*A*). To examine the role of eIF4E Ser209 phosphorylation in the hippocampus, we subjected wild-type and *Eif4e*^{Ser209Ala} phospho-mutant knock-in mice (4Eki) (Gkogkas et al., 2014) to hippocampus-dependent behavioral tests. First, we examined spatial memory in the Morris water maze task (MWM) (Fig. 1*B*). 4Eki mice were indistinguishable from wild-type mice during the learning phase, as they displayed comparable latency to find the hidden platform, and comparable numbers of platform crossings (Fig. 1*B*). Quadrant occupancy during the probe test on day 6 was not different between wild-type and 4Eki mice (Fig. 1*B*). Second, we assessed long-term contextual fear memory using a contextual fear conditioning (CFC) task (Fig. 1*C*). In line with MWM data, contextual memory was intact in 4Eki mice, as the percentage of freezing in response to context was not different from wild-type mice (Fig. 1*C*). These data indicate that hippocampus-dependent contextual memory is not affected by the lack of eIF4E phosphorylation.

We next measured long-term potentiation (LTP) in CA1 hippocampal area, a form of plasticity which is MAPK- and protein synthesis-dependent (Frey et al., 1988; English and Sweatt, 1997). Four trains of high frequency stimulation (4HFS) of the Schaffer collateral-CA1 synapses elicited long-lasting potentiation of field excitatory post-synaptic potentials (fEPSPs) in wild-type slices (Fig. 1*D*). The 4HFS-induced potentiation was not different in slices prepared from 4Eki mice, as compared to wild-type (Fig. *1D, E*). Altogether, mutating the single phosphorylation site on eIF4E (which lies downstream of the MAPK/ERK/MNK pathway and upstream of translation initiation) does not impair neither hippocampus-dependent learning and memory, nor CA1 hippocampal late-LTP.

Phospho-eIF4E regulates the translation of a subset of mRNAs

Given the unexpected result that eIF4E phosphorylation is not required for key forms of hippocampal memory formation and synaptic plasticity, we sought to elucidate the role of phospho-eIF4E in the brain by performing genome-wide analysis of mRNA translation, with the ribosome profiling methodology (Ingolia et al., 2012). Using forebrain tissue (including hippocampus) from wild-type and 4Eki mice, we generated libraries for RNA sequencing from randomly fragmented total RNA (a proxy for transcription) and from ribosome-protected footprints following RNAse digestion (a proxy for translation), to measure the

translational efficiency of mRNAs (Fig. 2*A*). We did not observe a significant change in global translation or transcription in 4Eki forebrain (Fig. 2*B*), in accordance with previous reports (Gkogkas et al., 2014). The high quality of footprint and mRNA libraries is evidenced first by the r^2 of Reads Per Kilobase of transcript per Million mapped reads (RPKM) between replicates, which is >0.99 for both footprints and total mRNA (Fig. 2-1*A*), second by the canonical distribution of footprint size (28-32nt) and of read distribution within the 3 frames (Fig. 2-1*B*) and third by Principal Components and Clustering Analysis of replicates (Fig. 2-1*C, D*). We found that even though the Ser209Ala mutation does not affect global translation, it regulates the translational efficiency of a subset of mRNAs (Fig. 2*B*). The translation of 651 mRNAs was significantly downregulated (4Eki/wild-type ratio ≤0.75, $p<0.05$), whereas the translation of 52 mRNAs was significantly upregulated (4Eki/wild-type ratio ≥1.5, $p<0.05$) (Fig. 2*B*).

Because UTRs harbor sequence elements, which may explain changes in translational efficiency, we analyzed 4Eki-sensitive mRNA 5′ and 3′ UTRs, along with 325 mRNAs (control group) that were not regulated by phospho-eIF4E in our ribosome profiling experiment (Fig. 2*C*), using the RegRNA suite (Huang et al., 2006). The 5′ UTRs of downregulated, but not upregulated mRNAs, contain a reduced number of upstream open reading frames (uORF), internal ribosome entry sites (IRES) and Terminal Oligopyrimidine Tract (TOP), as compared to the control group (Fig. 2*C*). The 3′ UTRs of downregulated mRNAs, but not of upregulated, harbor a significantly reduced number of Gamma interferon Activated Inhibitor of Translation (GAIT) elements, as compared to the control and upregulated mRNA groups (Fig. 2C). The incidence of Cytoplasmic Polyadenylation elements (CPE) both in downregulated and upregulated mRNAs is reduced, as compared to the control group (Fig. 2*C*). These data suggest that the incidence of 5′ uORF, IRES and 3′ GAIT elements in the UTRs of 4Eki downregulated mRNAs, as compared to upregulated and control groups, may reveal a previously unidentified phospho-eIF4E-dependent translational control mechanism in the brain. Notably, we analyzed the length and guanine-cytosine content (GC%) in UTRs, and detected a significant increase in the length of 5′ UTRs in downregulated mRNAs, as compared to other mRNA groups, but not for GC% (Fig. 2*D*). 3′ UTR length or GC% were not different between gene groups (Fig. 2*D*).

To further understand the translational control mechanisms downstream of phospho-eIF4E in the brain, we carried out gene-ontology analysis for the downregulated (Fig. 2*E, F, G)* and

upregulated genes (Fig. 2*H*). For the significantly downregulated genes group, we identified several biological process, molecular function and cellular component categories ($p<0.05$; Fig. 2*E, F*). Some key categories include response to stress, extracellular organization and extracellular matrix (ECM), biological adhesion and defense response, while some key pathways were also identified (such as PI3K-Akt signaling pathway and ECM-receptor interaction) (Fig. 2*E, F*). Some of the major gene groups that are downregulated in 4Eki forebrain are genes encoding for pituitary hormones and ECM genes (Fig. 2*G*), including *Mmp9*, which we have previously shown to be crucial for reversing behavioral, anatomical and biochemical deficits in *Fmr1*$^{-/y}$ mice (Gkogkas et al., 2014; Gantois et al., 2017). Conversely, in the upregulated genes group, the most enriched gene ontology category and pathway is the ribosome, while two major gene groups that are upregulated translationally include genes in the serotonin pathway and ribosomal protein coding genes (Fig. 2*H*). Taken together these data suggest that downstream of MAPK/ERK, eIF4E phosphorylation does not affect global translation, but preferentially regulates the synthesis of certain proteins by modulating their mRNA translation via 5′ and 3′ UTR elements, such as GAIT. Importantly, the list of regulated mRNAs points towards a role of phospho-eIF4E in ECM regulation, pituitary hormones, the serotonin pathway and ribosomal proteins.

Exaggerated inflammatory response and reduced serotonin levels in 4Eki brain

To further investigate the role of phospho-eIF4E in the brain, we proceeded to identify potential phenotypic changes, which could result from the aberrant translation of specific categories of mRNAs in 4Eki brain (Fig. 2). We hypothesized that inflammatory responses may be altered in 4Eki mice, given the known link of phospho-eIF4E and eIF4E to innate immunity (Colina et al., 2008; Herdy et al., 2012) and because many inflammatory mRNAs harbor GAIT elements in their 3′ UTRs (Mukhopadhyay et al., 2009), similarly to our upregulated mRNAs (Fig. 2*C*). The mRNA 3′ UTR GAIT element is a "gatekeeper" of inflammatory gene expression (Mukhopadhyay et al., 2009). Therefore, we set out to measure inflammatory reponses in forebrain lysates using quantitative ELISA for 6 major cytokines. Treatment of 4Eki mice with lipopolysaccharide (LPS; strain O111:B4, 5 mg/kg, intraperitoneally) led to a significantly higher expression of distinct cytokines 4 h post-injection in 4Eki mouse forebrain, as compared to wild-type (Fig. 3*A*). In 4Eki brain, we detected a significant increase in IL-2 (Interleukin-2) and TNFα (Tumor Necrosis Factor α) expression, both at baseline and following LPS stimulation, as compared to wild-type (Fig.

3*A*). For IFNγ (Interferon-γ), we detected a significant upregulation in 4Eki versus wild-type only following LPS stimulation, but not at baseline (Fig. 3*A*), while for IL-6, IL-10 and IL-1B there were no differences between 4Eki and wild-type mice (Fig. 3*A*). Interestingly, IL-2, TNFα and IFNγ are produced by Th1-type T-cell subsets, while IL-6, IL-10 and IL-1B by Th2-type (Romagnani, 2000).

We further reasoned that the translational upregulation of the serotonin uptake receptor (Slc6a4) and the enzyme tryptophan hydroxylase (Tph2) (Fig. 2*H*) would be accompanied by changes in the amount of serotonin in the 4Eki brain, as previously shown (Charoenphandhu et al., 2011; Zhang et al., 2012; Yohn et al., 2017). Using quantitative ELISA, we measured a decrease in tissue levels of serotonin in 4Eki forebrain, as compared to wild-type (Fig. 3*B*). Furthermore, we also detected an increase in Iba-1 (ionized calcium-binding adapter molecule-1) at baseline and following LPS stimulation in 4Eki mice, as compared to WT (Fig. 3*C*), suggesting that microglia are activated in the Ser209Ala mouse model.

Together, these data suggest that the elaborate translational landscape downstream of phospho-eIF4E elicits complex alterations in the brain consisting of changes in inflammatory responses and serotonergic function.

Depression and anxiety-like behaviors in 4Eki mice

There is a strong link between serotonin, pituitary hormones such as prolactin and depression/anxiety (Bob et al., 2007; Yohn et al., 2017). Moreover, phospho-eIF4E is upregulated in response to chronic treatment with the SSRI antidepressant fluoxetine (Dagestad et al., 2006). Thus, we reasoned that the pathways regulated by eIF4E phosphorylation could be linked to depression. To test this hypothesis, we subjected wild-type and 4Eki mice to the forced swim test (FST) and tail suspension test (TST), which have been shown to model depression-like behaviors in mice by assessing passive immobility after a few minutes of futile struggling (Cryan and Holmes, 2005). 4Eki mice remained immobile longer than wild-type mice in both FST and TST tests, suggesting a depression-like phenotype (Fig. 4*A*). To further study the depression-like phenotype of the 4Eki mice, we employed the Novelty-Supressed Feeding test (NSF), which measures the latency of a mouse to start feeding in a novel environment, following 24-h food restriction. It has been extensively shown that mouse models of depression display increased latencies to initiate

feeding in the NSF test (hyponeophagia) (Dulawa and Hen, 2005), while chronic anti-depressants were shown to reduce this latency(Britton and Britton, 1981). 4Eki mice required a significantly higher amount of time per session to initiate feeding in NSF, as compared to WT (Fig. 3*A*). Furthermore, we examined 4Eki mice for anxiety-like behaviors using the open field (OF) test (Fig. 4*B*). 4Eki mice spent significantly less time in the central region of the arena, and significantly more time in proximity to walls or corners, suggesting elevated anxiety, however the time spent outside the central square and total distance travelled were similar between 4Eki and wild-type mice, indicating that locomotion was not affected (Fig. 4*B*). In line with these findings, we detected an anxiety-like phenotype in 4Eki mice subjected to the Elevated Plus Maze test (EPM; Fig. 4*C*). 4Eki mice, as compared to wild-type, spend significantly less time in the open and significantly more time in the closed arms of the maze (Fig. 3*C*). In summary, these data indicate that 4Eki mice display anxiety and depression-like behaviors.

Chronic fluoxetine treatment does not rescue depression-like behaviors in 4Eki mice

Chronic fluoxetine treatment induced phosphorylation of eIF4E at Ser209 (Dagestad et al., 2006) and alleviated depression-like phenotypes in mice (Dulawa et al., 2004). Thus, we hypothesized that the chronic anti-depressant effect of fluoxetine is mediated via stimulation of eIF4E phosphorylation (Fig. 5*A*). Chronic (21 d) intraperitoneal treatment of wild-type mice with fluoxetine (10 mg/kg/day) led to a ~25% decrease in immobility in both FST and TST tests (Fig. 5A, *B, C*), which is in accordance with previous reports (Dulawa et al., 2004). Strikingly, in 4Eki mice fluoxetine did not affect immobility in both tests (Fig. 5*B, C*), indicating that phospho-eIF4E is required for the antidepressant action of fluoxetine.

Reduced cap-binding of rpL13a and eIF4A1 in 4Eki mice

UTR analysis of differentially translated mRNAs in the forebrain of 4Eki mice revealed that upregulated mRNAs display a higher incidence of 3′ UTR GAIT elements, as compared to downregulated mRNAs (Fig. 2*C*). GAIT elements repress translation by recruiting a complex of proteins (GAIT complex: rpL13a, Eprs and Gapdh) on mRNA 3′ UTR (Mukhopadhyay et al., 2009). Subsequently, the GAIT complex is bridged to the 5′ UTR cap-bound eIF4F, via direct interaction of the GAIT complex protein rpL13a and eIF4G (Fig. 6*A*). Reduced binding of GAIT complexes to eIF4F when phospho-eIF4E is depleted, could explain the upregulation of a small subset of mRNAs containing 3′ UTR GAIT elements (52; Fig. *2C, H*) via translational disinhibition. Likewise, mRNAs with low incidence of 3′ UTR GAIT

elements should not be affected to the same extent by this regulatory mechanism (Fig. *2C, G*). To test this hypothesis, we carried out cap-column pulldown of forebrain lysates using m^7GDP agarose beads, followed by immunoblotting of cap-bound and of whole lysates as a control (Fig. 6*A*). By probing for key eIF4F proteins (eIF4E, eIF4G and eIF4A), we can detect changes in their binding to the mRNA cap. By probing for the GAIT complex proteins rpL13a, Eprs and Gapdh in cap-bound fractions, we can assess changes in GAIT complex-eIF4F binding; importantly rpL13a bridges GAIT to eIF4F (Fig. 6*A*). We detected in 4Eki forebrain lysates, decreased cap binding of rpL13a and of the eIF4F helicase eIF4A1, while eIF4E, eIF4G, Eprs and Gapdh cap binding was not altered (Fig. 6*A, B*). Eprs and Gapdh cap-binding was not altered in 4Eki mice, which could be due to the fact that these proteins may interact with eIF4F as monomers, outside of the GAIT complex (Sampath et al., 2004). This is not the case for ribosomal protein rpL13a, as its main extra-ribosomal function is to bridge GAIT to eIF4F and mediate translational repression (Kapasi et al., 2007).

Thus, ablation of the single phosphorylation site on eIF4E engenders selective translation of a subset of mRNAs, conceivably through altered cap-binding and translation initiation mediated by mRNA UTR elements, such as GAIT (Fig. 7*A*).

Discussion (1417 words)

We show that phospho-eIF4E plays a previously unidentified role in the brain, whereby its depletion engenders depression-like behaviors (Fig. 4) and resistance to the chronic anti-depressant action of the SSRI fluoxetine (Fig. 7*B*). We also show that eIF4E phosphorylation is not required for major forms of hippocampal learning and memory and L-LTP (Fig. 1). We further demonstrate that a potential underlying mechanism involves the selective mRNA translation of GAIT element-containing mRNAs and of mRNAs harboring long 5′ UTRs (Fig. 7*A*). This multifaceted translational control pathway in 4Eki mouse brain may be responsible for the observed changes in inflammatory responses, serotonin levels, pituitary hormones and the ECM (Fig. 2, 3), which could underlie the depression-like behaviors (Fig. 4) and the resistance to the antidepressant action of fluoxetine (Fig. 5).

Translational control by the MAPK pathway was shown to be crucial for hippocampal synaptic plasticity, learning and memory (Kelleher et al., 2004). Contrary to the prediction that ablation of phospho-Ser209 in eIF4E would recapitulate MAPK deletion phenotypes, we found that in Ser209Ala mutant mice (4Eki), hippocampal learning and memory, as well as a

major form of long-term synaptic plasticity (L-LTP) are intact (Fig. 1). It is generally believed that L-LTP and long-term memory require new protein synthesis (Frey et al., 1988). We show for the first time that the phosphorylation of eIF4E downstream of MAPK/ERK is not required for L-LTP (Fig. 1*D*). We cannot rule out the possibility that phospho-eIF4E is essential for other forms of synaptic plasticity (Panja et al., 2014) or that it is important in brain regions outside the hippocampus. We also cannot exclude the presence of compensatory mechanisms in 4Eki mice, (such as mTORC1 activation), which could substitute for the loss of eIF4E phosphorylation. Alternatively, MAPK/ERK may regulate hippocampal synaptic plasticity, learning and memory by phosphorylating other translation initiation factors.

Ribosome profiling in the brain of 4Eki mice revealed translational downregulation of several mRNAs (encoding for ECM genes and pituitary hormones) (Fig. 2*G*). eIF4E phosphorylation was previously suggested to control cancer metastasis (Furic et al., 2010; Robichaud et al., 2015), by controlling ECM function and in particular the translation of MMPs, such as MMP-9 (Furic et al., 2010; Gkogkas et al., 2014; Gantois et al., 2017). Thus, it will be important to further investigate the role of ECM regulation downstream of phospho-eIF4E in the brain. Control of pituitary mRNA translation is a novel function assigned to phospho-eIF4E, and apart from its link to depression, it will be important to examine its potential links to other neuropsychiatric or neurodevelopmental disorders or cancer (such as pituitary adenomas). On the other hand, serotonin pathway and ribosomal protein coding genes are upregulated in 4Eki brain (Fig. 2*H*). Given the interplay between the hypothalamic–pituitary–adrenal axis, serotonin and dopamine (Hamon and Blier, 2013; Hoogendoorn et al., 2017), we are proposing a new translational control pathway (via phospho-eIF4E) implicated in this regulation, which may be modulated pharmacologically. The ribosome profiling strategy was invaluable in identifying phospho-eIF4E-regulated transcripts, and subsequently phenotypic changes. However, it did not reveal cell-type specific alterations in translation, which could further elucidate the mechanisms underlying the depression-like phenotypes observed in 4Eki mice. Given that we detected inflammatory changes in Iba-1 (a marker of microglia activation; Fig. 3*C*), it would be imperative to carry out cell-type specific profiling of translation in neuronal and non-neuronal cells (e.g. microglia) using methodologies such as TRAP (Heiman et al., 2014). Nevertheless, our translational profiling revealed that ablation of eIF4E phosphorylation downregulates the translation of a large subset of mRNAs, without affecting global translation, and, upregulates the translation of a very small subset of mRNAs

(Fig. 2). Overall, these data suggest that eIF4E phosphorylation promotes translation initiation.

Pro-inflammation programs in 4Eki mice (Fig. 2, 3) could be causal for the depression-like behaviors observed in these mice (Fig. 4). Depression is frequently comorbid with many inflammatory illnesses (Liu et al., 2017), while antidepressants can decrease inflammatory responses (Wiedlocha et al., 2017), suggesting that depression and inflammation are closely linked. Conceivably, pro-inflammatory responses in 4Eki brain could be linked to depression-like behaviors either: a) by GAIT mRNA translational disinhibition (Fig. 2, 6), linked to inflammation (Fig. 3), or b) through the known link of eIF4E and enhanced type-I interferon production (Colina et al., 2008) or c) as a result of enhanced activity of NF-κB following translational downregulation of its inhibitor IκBα in 4Eki (Herdy et al., 2012). Indeed, we observed a baseline and LPS-stimulated upregulation of Th1-type (Romagnani, 2000) cytokines: IFNγ, TNFα and IL-2 (Fig. 3*A*). Notably, a shift in the Th1/Th2 balance in favor of Th1 cytokine expression cytokines was shown to be linked to depression (Gabbay et al., 2009; Maes, 2011) and other neuropsychiatric disorders (Hickie and Lloyd, 1995).

We identified exacerbated immobility/"despair-like", hyponeophagy and anxiety-like behaviors in 4Eki mice, which are reminiscent of human depression/anxiety (Fig. 4). The link between phospho-eIF4E and depression is further strengthened by the fact that chronic fluoxetine treatment (10 mg/kg for 21d) requires eIF4E phosphorylation to exert its anti-depressant effect (Fig. 5). Fluoxetine also recruits other pathways upstream of the translation initiation machinery, such as mTORC1 (Liu et al., 2015). While the connection between inflammation and depression is still under investigation, our data highlight a new translational control pathway, which may underlie the chronic antidepressant action of SSRIs and could be exploited to design novel antidepressants by boosting eIF4E phosphorylation (Fig. 7*C*).

In addition, we have further elucidated the mechanism of translational control downstream of phospho-eIF4E by identifying key 5′ and 3′ UTR sequence elements, and changes in signaling which may confer specificity to phospho-eIF4E translational control (Fig. 2*C*). From the UTR analysis, we identified an underrepresentation of uORF, IRES, TOP, CPE and GAIT elements in 4Eki downregulated mRNAs. CPE elements may regulate translation of

4Eki-sensitive mRNAs, which could be explained through changes in the activity of Poly(A)-binding protein (PABP), which prompts mRNA circularization by bridging 5′ eIF4G to 3′ poly(A) tail (Smith et al., 2014). Furthermore, translation of uORF-containing mRNAs is regulated by the eIF2α pathway in the brain (Costa-Mattioli et al., 2007). Even though we did not detect any changes in eIF2α phosphorylation in 4Eki mice (data not shown), mTORC1 may regulate uORF-containing mRNA translation (Schepetilnikov et al., 2013). Likewise, we did not detect significant changes in IRES translation in 4Eki mice (data not shown). The translation of TOP mRNAs (such as ribosomal protein coding mRNAs) was previously shown to be mTORC1-sensitive (Avni et al., 1997; Thoreen et al., 2012), which is in line with our GO analysis (Fig. 2*G*, *H*; KEGG pathways).

The presence of GAIT sequence elements in the 3′ UTR of pro-inflammatory mRNAs suppresses their translation (Mukhopadhyay et al., 2008). A key event in this process is the binding of rpL13a, a core constituent of the GAIT protein complex, to the 5′ cap by direct binding to eIF4G (Fox, 2015). Genetic depletion of eIF4E Ser209 phosphorylation leads to reduced binding of rpL13a to the 5′ cap (Fig. 6), predicting that in 4Eki brain there would be translational disinhibition of mRNAs harboring GAIT elements. Indeed, 4Eki-downregulated mRNAs have a low incidence of 3′ UTR GAIT elements, which could explain why they are not affected by phospho-eIF4E-mediated, GAIT complex-dependent translational disinhibition. This also suggests that downregulation of the 651 mRNAs probably occurs via a different mechanism. Conversely, upregulated mRNAs display a significantly higher incidence of 3′ UTR GAIT elements (Fig. 2*C*). Concomitantly, 4Eki brains exhibit exaggerated expression of pro-inflammatory cytokines, which could be explained by GAIT complex-mediated disinhibition of mRNAs coding for cytokines (Fig. 3*A*). Furthermore, cap-pulldown of the helicase eIF4A1 is significantly reduced in 4Eki forebrain (Fig. 6), and is accompanied by increased length of 5′ UTRs in 4Eki downregulated mRNAs, as compared to other groups (Fig. 2*D*). Thus, it is possible that phospho-eIF4E requires the helicase eIF4A1 to resolve long 5′ UTRs, which is in accordance with previous reports linking eIF4E to eIF4A1 activity (Feoktistova et al., 2013). This mechanism could explain the translational downregulation of the 651 mRNAs. Thus, our ribosome profiling data along with the biochemical investigation of cap complex formation in the brains of 4Eki mice have revealed potential mechanisms for the observed selective translational control. However, further work

is required to build a comprehensive model for the synergistic action of UTR elements such as GAIT, uORF, IRES, TOP and CPE, downstream of eIF4E phosphorylation.

In conclusion, phospho-eIF4E-dependent translation of GAIT element-containing mRNAs may constitute a unifying mechanistic explanation as to how dysregulated translational control of specific mRNAs could be causal for inflammation and depression, without affecting general translation.

References

Atkins CM, Selcher JC, Petraitis JJ, Trzaskos JM, Sweatt JD (1998) The MAPK cascade is required for mammalian associative learning. Nature neuroscience 1:602-609.

Avni D, Biberman Y, Meyuhas O (1997) The 5' terminal oligopyrimidine tract confers translational control on TOP mRNAs in a cell type- and sequence context-dependent manner. Nucleic acids research 25:995-1001.

Bob P, Fedor-Freybergh PG, Susta M, Pavlat J, Jasova D, Zima T, Benakova H, Miklosko J, Hynek K, Raboch J (2007) Depression, prolactin and dissociated mind. Neuro Endocrinol Lett 28:639-642.

Bramham CR, Jensen KB, Proud CG (2016) Tuning Specific Translation in Cancer Metastasis and Synaptic Memory: Control at the MNK-eIF4E Axis. Trends Biochem Sci 41:847-858.

Britton DR, Britton KT (1981) A sensitive open field measure of anxiolytic drug activity. Pharmacol Biochem Behav 15:577-582.

Cao R, Gkogkas CG, de Zavalia N, Blum ID, Yanagiya A, Tsukumo Y, Xu H, Lee C, Storch KF, Liu AC, Amir S, Sonenberg N (2015) Light-regulated translational control of circadian behavior by eIF4E phosphorylation. Nature neuroscience 18:855-862.

Charoenphandhu J, Teerapornpuntakit J, Nuntapornsak A, Krishnamra N, Charoenphandhu N (2011) Anxiety-like behaviors and expression of SERT and TPH in the dorsal raphe of estrogen- and fluoxetine-treated ovariectomized rats. Pharmacol Biochem Behav 98:503-510.

Colina R, Costa-Mattioli M, Dowling RJ, Jaramillo M, Tai LH, Breitbach CJ, Martineau Y, Larsson O, Rong L, Svitkin YV, Makrigiannis AP, Bell JC, Sonenberg N (2008) Translational control of the innate immune response through IRF-7. Nature 452:323-328.

Costa-Mattioli M, Gobert D, Stern E, Gamache K, Colina R, Cuello C, Sossin W, Kaufman R, Pelletier J, Rosenblum K, Krnjevic K, Lacaille JC, Nader K, Sonenberg N (2007) eIF2alpha phosphorylation bidirectionally regulates the switch from short- to long-term synaptic plasticity and memory. Cell 129:195-206.

Cryan JF, Holmes A (2005) The ascent of mouse: advances in modelling human depression and anxiety. Nat Rev Drug Discov 4:775-790.

Dagestad G, Kuipers SD, Messaoudi E, Bramham CR (2006) Chronic fluoxetine induces region-specific changes in translation factor eIF4E and eEF2 activity in the rat brain. The European journal of neuroscience 23:2814-2818.

Dulawa SC, Hen R (2005) Recent advances in animal models of chronic antidepressant effects: the novelty-induced hypophagia test. Neurosci Biobehav Rev 29:771-783.

Dulawa SC, Holick KA, Gundersen B, Hen R (2004) Effects of chronic fluoxetine in animal models of anxiety and depression. Neuropsychopharmacology 29:1321-1330.

English JD, Sweatt JD (1997) A requirement for the mitogen-activated protein kinase cascade in hippocampal long term potentiation. The Journal of biological chemistry 272:19103-19106.

Feoktistova K, Tuvshintogs E, Do A, Fraser CS (2013) Human eIF4E promotes mRNA restructuring by stimulating eIF4A helicase activity. Proceedings of the National Academy of Sciences of the United States of America 110:13339-13344.

Flynn A, Proud CG (1995) Serine 209, not serine 53, is the major site of phosphorylation in initiation factor eIF-4E in serum-treated Chinese hamster ovary cells. The Journal of biological chemistry 270:21684-21688.

Fox PL (2015) Discovery and investigation of the GAIT translational control system. RNA 21:615-618.

Frey U, Krug M, Reymann KG, Matthies H (1988) Anisomycin, an inhibitor of protein synthesis, blocks late phases of LTP phenomena in the hippocampal CA1 region in vitro. Brain research 452:57-65.

Furic L, Rong L, Larsson O, Koumakpayi IH, Yoshida K, Brueschke A, Petroulakis E, Robichaud N, Pollak M, Gaboury LA, Pandolfi PP, Saad F, Sonenberg N (2010) eIF4E phosphorylation promotes tumorigenesis and is associated with prostate cancer progression. Proceedings of the National Academy of Sciences of the United States of America 107:14134-14139.

Gabbay V, Klein RG, Alonso CM, Babb JS, Nishawala M, De Jesus G, Hirsch GS, Hottinger-Blanc PM, Gonzalez CJ (2009) Immune system dysregulation in adolescent major depressive disorder. Journal of affective disorders 115:177-182.

Gantois I et al. (2017) Metformin ameliorates core deficits in a mouse model of fragile X syndrome. Nature medicine 23:674-677.

Gkogkas CG, Khoutorsky A, Cao R, Jafarnejad SM, Prager-Khoutorsky M, Giannakas N, Kaminari A, Fragkouli A, Nader K, Price TJ, Konicek BW, Graff JR, Tzinia AK, Lacaille JC, Sonenberg N (2014) Pharmacogenetic inhibition of eIF4E-dependent Mmp9 mRNA translation reverses fragile X syndrome-like phenotypes. Cell reports 9:1742-1755.

Hamon M, Blier P (2013) Monoamine neurocircuitry in depression and strategies for new treatments. Prog Neuropsychopharmacol Biol Psychiatry 45:54-63.

Heiman M, Kulicke R, Fenster RJ, Greengard P, Heintz N (2014) Cell type-specific mRNA purification by translating ribosome affinity purification (TRAP). Nat Protoc 9:1282-1291.

Herdy B et al. (2012) Translational control of the activation of transcription factor NF-kappaB and production of type I interferon by phosphorylation of the translation factor eIF4E. Nature immunology 13:543-550.

Hickie I, Lloyd A (1995) Are cytokines associated with neuropsychiatric syndromes in humans? Int J Immunopharmacol 17:677-683.

Hinnebusch AG, Ivanov IP, Sonenberg N (2016) Translational control by 5'-untranslated regions of eukaryotic mRNAs. Science 352:1413-1416.

Hoogendoorn CJ, Roy JF, Gonzalez JS (2017) Shared Dysregulation of Homeostatic Brain-Body Pathways in Depression and Type 2 Diabetes. Curr Diab Rep 17:90.

Huang HY, Chien CH, Jen KH, Huang HD (2006) RegRNA: an integrated web server for identifying regulatory RNA motifs and elements. Nucleic acids research 34:W429-434.

Ingolia NT, Brar GA, Rouskin S, McGeachy AM, Weissman JS (2012) The ribosome profiling strategy for monitoring translation in vivo by deep sequencing of ribosome-protected mRNA fragments. Nat Protoc 7:1534-1550.

764 Joshi B, Cai AL, Keiper BD, Minich WB, Mendez R, Beach CM, Stepinski J, Stolarski R,
765 Darzynkiewicz E, Rhoads RE (1995) Phosphorylation of eukaryotic protein synthesis
766 initiation factor 4E at Ser-209. The Journal of biological chemistry 270:14597-14603.
767 Joshi S, Platanias LC (2014) Mnk kinase pathway: Cellular functions and biological
768 outcomes. World J Biol Chem 5:321-333.
769 Kanterewicz BI, Urban NN, McMahon DB, Norman ED, Giffen LJ, Favata MF, Scherle PA,
770 Trzskos JM, Barrionuevo G, Klann E (2000) The extracellular signal-regulated kinase
771 cascade is required for NMDA receptor-independent LTP in area CA1 but not area
772 CA3 of the hippocampus. The Journal of neuroscience : the official journal of the
773 Society for Neuroscience 20:3057-3066.
774 Kapasi P, Chaudhuri S, Vyas K, Baus D, Komar AA, Fox PL, Merrick WC, Mazumder B
775 (2007) L13a blocks 48S assembly: role of a general initiation factor in mRNA-
776 specific translational control. Mol Cell 25:113-126.
777 Kelleher RJ, 3rd, Govindarajan A, Jung HY, Kang H, Tonegawa S (2004) Translational
778 control by MAPK signaling in long-term synaptic plasticity and memory. Cell
779 116:467-479.
780 Knauf U, Tschopp C, Gram H (2001) Negative regulation of protein translation by mitogen-
781 activated protein kinase-interacting kinases 1 and 2. Molecular and cellular biology
782 21:5500-5511.
783 Konicek BW, Stephens JR, McNulty AM, Robichaud N, Peery RB, Dumstorf CA, Dowless
784 MS, Iversen PW, Parsons S, Ellis KE, McCann DJ, Pelletier J, Furic L, Yingling JM,
785 Stancato LF, Sonenberg N, Graff JR (2011) Therapeutic inhibition of MAP kinase
786 interacting kinase blocks eukaryotic initiation factor 4E phosphorylation and
787 suppresses outgrowth of experimental lung metastases. Cancer research 71:1849-
788 1857.
789 Lachance PE, Miron M, Raught B, Sonenberg N, Lasko P (2002) Phosphorylation of
790 eukaryotic translation initiation factor 4E is critical for growth. Molecular and cellular
791 biology 22:1656-1663.
792 Liu XL, Luo L, Mu RH, Liu BB, Geng D, Liu Q, Yi LT (2015) Fluoxetine regulates mTOR
793 signalling in a region-dependent manner in depression-like mice. Scientific reports
794 5:16024.
795 Liu YZ, Wang YX, Jiang CL (2017) Inflammation: The Common Pathway of Stress-Related
796 Diseases. Front Hum Neurosci 11:316.
797 Maes M (2011) Depression is an inflammatory disease, but cell-mediated immune activation
798 is the key component of depression. Prog Neuropsychopharmacol Biol Psychiatry
799 35:664-675.
800 McKendrick L, Morley SJ, Pain VM, Jagus R, Joshi B (2001) Phosphorylation of eukaryotic
801 initiation factor 4E (eIF4E) at Ser209 is not required for protein synthesis in vitro and
802 in vivo. Eur J Biochem 268:5375-5385.
803 Mukhopadhyay R, Jia J, Arif A, Ray PS, Fox PL (2009) The GAIT system: a gatekeeper of
804 inflammatory gene expression. Trends Biochem Sci 34:324-331.
805 Mukhopadhyay R, Ray PS, Arif A, Brady AK, Kinter M, Fox PL (2008) DAPK-ZIPK-L13a
806 axis constitutes a negative-feedback module regulating inflammatory gene expression.
807 Mol Cell 32:371-382.
808 Panja D, Kenney JW, D'Andrea L, Zalfa F, Vedeler A, Wibrand K, Fukunaga R, Bagni C,
809 Proud CG, Bramham CR (2014) Two-stage translational control of dentate gyrus LTP
810 consolidation is mediated by sustained BDNF-TrkB signaling to MNK. Cell Rep
811 9:1430-1445.

Pyronnet S, Imataka H, Gingras AC, Fukunaga R, Hunter T, Sonenberg N (1999) Human eukaryotic translation initiation factor 4G (eIF4G) recruits mnk1 to phosphorylate eIF4E. The EMBO journal 18:270-279.

Quackenbush J (2002) Microarray data normalization and transformation. Nature genetics 32 Suppl:496-501.

Reimand J, Arak T, Adler P, Kolberg L, Reisberg S, Peterson H, Vilo J (2016) g:Profiler-a web server for functional interpretation of gene lists (2016 update). Nucleic acids research 44:W83-89.

Reiner A, Yekutieli D, Benjamini Y (2003) Identifying differentially expressed genes using false discovery rate controlling procedures. Bioinformatics 19:368-375.

Robichaud N, del Rincon SV, Huor B, Alain T, Petruccelli LA, Hearnden J, Goncalves C, Grotegut S, Spruck CH, Furic L, Larsson O, Muller WJ, Miller WH, Sonenberg N (2015) Phosphorylation of eIF4E promotes EMT and metastasis via translational control of SNAIL and MMP-3. Oncogene 34:2032-2042.

Romagnani S (2000) T-cell subsets (Th1 versus Th2). Ann Allergy Asthma Immunol 85:9-18; quiz 18, 21.

Sampath P, Mazumder B, Seshadri V, Gerber CA, Chavatte L, Kinter M, Ting SM, Dignam JD, Kim S, Driscoll DM, Fox PL (2004) Noncanonical function of glutamyl-prolyl-tRNA synthetase: gene-specific silencing of translation. Cell 119:195-208.

Schafe GE, Atkins CM, Swank MW, Bauer EP, Sweatt JD, LeDoux JE (2000) Activation of ERK/MAP kinase in the amygdala is required for memory consolidation of pavlovian fear conditioning. The Journal of neuroscience : the official journal of the Society for Neuroscience 20:8177-8187.

Schepetilnikov M, Dimitrova M, Mancera-Martinez E, Geldreich A, Keller M, Ryabova LA (2013) TOR and S6K1 promote translation reinitiation of uORF-containing mRNAs via phosphorylation of eIF3h. The EMBO journal 32:1087-1102.

Smith RW, Blee TK, Gray NK (2014) Poly(A)-binding proteins are required for diverse biological processes in metazoans. Biochem Soc Trans 42:1229-1237.

Sonenberg N, Hinnebusch AG (2009) Regulation of translation initiation in eukaryotes: mechanisms and biological targets. Cell 136:731-745.

Thomas GM, Huganir RL (2004) MAPK cascade signalling and synaptic plasticity. Nature reviews Neuroscience 5:173-183.

Thoreen CC, Chantranupong L, Keys HR, Wang T, Gray NS, Sabatini DM (2012) A unifying model for mTORC1-mediated regulation of mRNA translation. Nature 485:109-113.

Wiedlocha M, Marcinowicz P, Krupa R, Janoska-Jazdzik M, Janus M, Debowska W, Mosiolek A, Waszkiewicz N, Szulc A (2017) Effect of antidepressant treatment on peripheral inflammation markers - A meta-analysis. Prog Neuropsychopharmacol Biol Psychiatry.

Yates A et al. (2016) Ensembl 2016. Nucleic acids research 44:D710-716.

Yohn CN, Gergues MM, Samuels BA (2017) The role of 5-HT receptors in depression. Mol Brain 10:28.

Zhang J, Fan Y, Li Y, Zhu H, Wang L, Zhu MY (2012) Chronic social defeat up-regulates expression of the serotonin transporter in rat dorsal raphe nucleus and projection regions in a glucocorticoid-dependent manner. Journal of neurochemistry 123:1054-1068.

Zhu JJ, Qin Y, Zhao M, Van Aelst L, Malinow R (2002) Ras and Rap control AMPA receptor trafficking during synaptic plasticity. Cell 110:443-455.

Legends

Figure 1 Intact spatial learning and memory, contextual fear memory and L-LTP in 4Eki mice A. Representative confocal images of immunofluorescent staining of wild-type dorsal hippocampi with antibodies against total and phospho-Ser209 eIF4E; white scale bar 100 μm **B.** Morris water maze (MWM) task. Left: graphic depiction of experimental design; latency (s) to find hidden platform during experimental days. Right: Platform Crossings and Quadrant occupancy during probe test (WT n=7, 4Eki n=8); Repeated measures ANOVA, with Tukey's post-hoc ***$p<0.001$. **C.** Contextual Fear Conditioning in 4Eki mice. Percentage freezing 24 h after initial shock (WT n=8, 4Eki n=8); Student's *t*-test. **D.** CA1 late-LTP (L-LTP) recordings in 4Eki mice. Normalized fEPSP slope over time (min) for 240 min. **E.** Summary quantification of percentage potentiation for L-LTP. Student's *t*-test; **$p<0.01$.

Figure 2 Ribosome profiling reveals preferential translation of a subset of mRNAs in the forebrain of 4Eki mice. A. Experimental design to assess genome-wide translational efficiency of mRNAs using ribosome profiling in whole brain tissue from WT and 4Eki mice. **B.** $\log_2$Translational Efficiency (TE) Plot showing translationally upregulated (red), downregulated (blue) and control (grey) mRNAs in 4Eki versus WT libraries ($p<0.05$ and $0.75 \geq TE\ ratio \leq 1.5$; grey depicts unchanged mRNAs; n=2 for footprints and mRNA). **C.** UTR analysis using RegRNA in downregulated (651; blue), upregulated (52; red) and control (325; grey) mRNAs in 4Eki, as compared to wild-type. Percentage of genes containing one or more of the depicted RNA sequence elements in 5′ or 3′UTR is shown; # marks categories in downregulated or upregulated mRNAs which are underrepresented, as compared to control mRNAs. **D.** Length and GC content analysis of differentially translated mRNAs. Length (bp) or percentage of GC content are displayed for 5′ (left) or 3′ UTR (right); # corresponds to $p<0.05$ difference from all other categories – all other multiple comparisons between groups are not-significant; One-way ANOVA with Tukey's post-hoc. **E.** Gene ontology analysis of 651 downregulated genes; plots for biological process, molecular function and cellular component with number of genes in each category and p-values next to each category are shown. **F.** KEGG pathway analysis for downregulated genes. **G.** Major genes downregulated in ribosome profiling organized in two categories: pituitary hormone genes and ECM genes with p-value and FDR. **H.** Gene ontology analysis of 52 upregulated genes; plots for cellular component with number of genes in each category and p-values and KEGG pathway analysis. Major genes upregulated in ribosome profiling organized in two categories:

894 serotonin and ribosomal proteins; p-value and FDR are shown for downregulated and
895 upregulated genes.
896
897 **Figure 2-1 Reproducibility and quality of RPF data. A.** Reproducibility plots for WT and
898 4Eki sequenced libraries (for replicates of total mRNA and footprints (grey corresponds to
899 data points with >128 reads). **B.** Frequency and length of mapped reads and fraction of reads
900 within start codon window for the 3 frames for total mRNA and footprint libraries. Principle
901 components analysis (PCA) and clustering analysis dendrogram for **C.** Translation and **D.**
902 Transcription for the two biological replicates used for WT (WT1, WT2) or 4Eki (KI1, KI2).
903
904 **Figure 3 Exaggerated inflammatory responses and reduced serotonin levels in 4Eki**
905 **brain. A.** Quantitative ELISA for 6 mouse inflammatory cytokines in WT and 4Eki
906 forebrains (n=10 for each genotype). Th1 cytokines are depicted in blue and Th2 in grey. **B.**
907 Left: Serotonin pathway genes upregulated in 4Eki brain (marked in red). Quantitative
908 ELISA for serotonin (5-HT) in WT and 4Eki forebrains (n=20 for each genotype).
909 Normalized concentration (pg/mg) is shown for all experiments. **C.** Quantitative ELISA for
910 Iba-1, a marker of activated microglia (n=10 for each genotype). For A and C: One-way
911 ANOVA with Bonferroni's post-hoc; ***p<0.001, **p<0.01. For C: Student's *t*-test;
912 ***p<0.001.
913
914 **Figure 4 Depression and anxiety-like behaviors in 4Eki mice. A.** Immobility time (s) as an
915 indicator of depression-like behaviors in left: forced swimming test (FST) and middle: tail
916 suspension test (TST) in WT (n=14) and 4Eki (n=18) mice. Right: Latency to start feeding in
917 a novel environment, as a proxy for depression/anxiety mediated hypophagia in WT and 4Eki
918 (n=18 each) mice using the Novelty suppressed feeding test (NSF). **B.** Open field
919 exploration test in WT (n=10) and 4EKI (n=12) mice, as a measure of anxiety. Time (s) spent
920 in the center square, in proximity of corners or walls or outside the center square and total
921 distance travelled are shown. For A and B: Student's *t*-test; *p<0.05, **p<0.01 and
922 ***p<0.001. **C.** Elevated Plus Maze test in WT (n=8) and 4EKI (n=8) mice, as a measure of
923 anxiety. Time (s) spent in the open or closed arms of the elevated maze is shown. For C:
924 One-way ANOVA with Bonferroni's post-hoc; ***p<0.001.
925
926 **Figure 5 Chronic fluoxetine intraperitoneal treatment does not reverse depression-like**
927 **behaviors in 4Eki mice. A.** Outline of chronic fluoxetine regimen. Intraperitoneal injection

of 10 mg/kg/d for 21 days reduces immobility time (s) in WT (n=12) but not 4Eki (n=12) mice **B.** in the forced swimming (FST) **C.** and tail suspension (TST) tests. Student's *t*-test; *p<0.05, **p<0.01, ***p<0.001.

Figure 6 Altered cap-binding of GAIT complex protein rpL13a and eIF4A1 in 4Eki brains. A. Cap-column (m^7GDP) pulldown from forebrain lysates (WT and 4Eki; n=4 per genotype or n=8 for Eprs, Gapdh). Left: A cartoon of the closed loop model of translation depicting binding of repressive 3′ UTR GAIT elements to 5′ UTR cap-bound eIF4F complex, via rpL13a and below a depiction of a cap-column agarose bead. Representative immunoblot images from cap-bound and input lysates probed with antibodies against the indicated proteins (eIF4E, eIF4G, eIF4A1 rpL13a, Eprs and Gapdh; β-actin is the loading control). **B.** Quantification of protein expression from input (5%) and cap-bound lysates. Protein expression (arbitrary units) normalized to input protein expression for cap-bound lysates and to *β*-actin for input lysates. Student's *t*-test; *p<0.05

Figure 7 Depletion of eIF4E phosphorylation engenders inflammatory and depression-like phenotypes via selective translational control of a subset of mRNAs. A. Ablation of the single phosphorylation site on eIF4E (Ser209→Ala) does not affect global protein synthesis, but rather the translation of a subset of mRNAs harboring GAIT elements, which engenders a depression-like phenotype in 4Eki mice. 4Eki mice also display increased expression of inflammatory cytokines, which could be linked to disinhibition of GAIT translational repression and possibly to depression-like phenotypes. Altered cap binding of the helicase eIF4A1 and/or of the GAIT complex protein rpL13a could be the mechanism underlying altered translation initiation following depletion of Ser209 eIF4E phosphorylation. **B.** The SSRI fluoxetine requires eIF4E phosphorylation to exert its antidepressant action. **C.** Phosphorylation of eIF4E promotes anti-inflammatory and antidepressant pathways.

Illustrations and Tables

Table 1 Details of Antibodies used

Table 2 Statistical Analysis

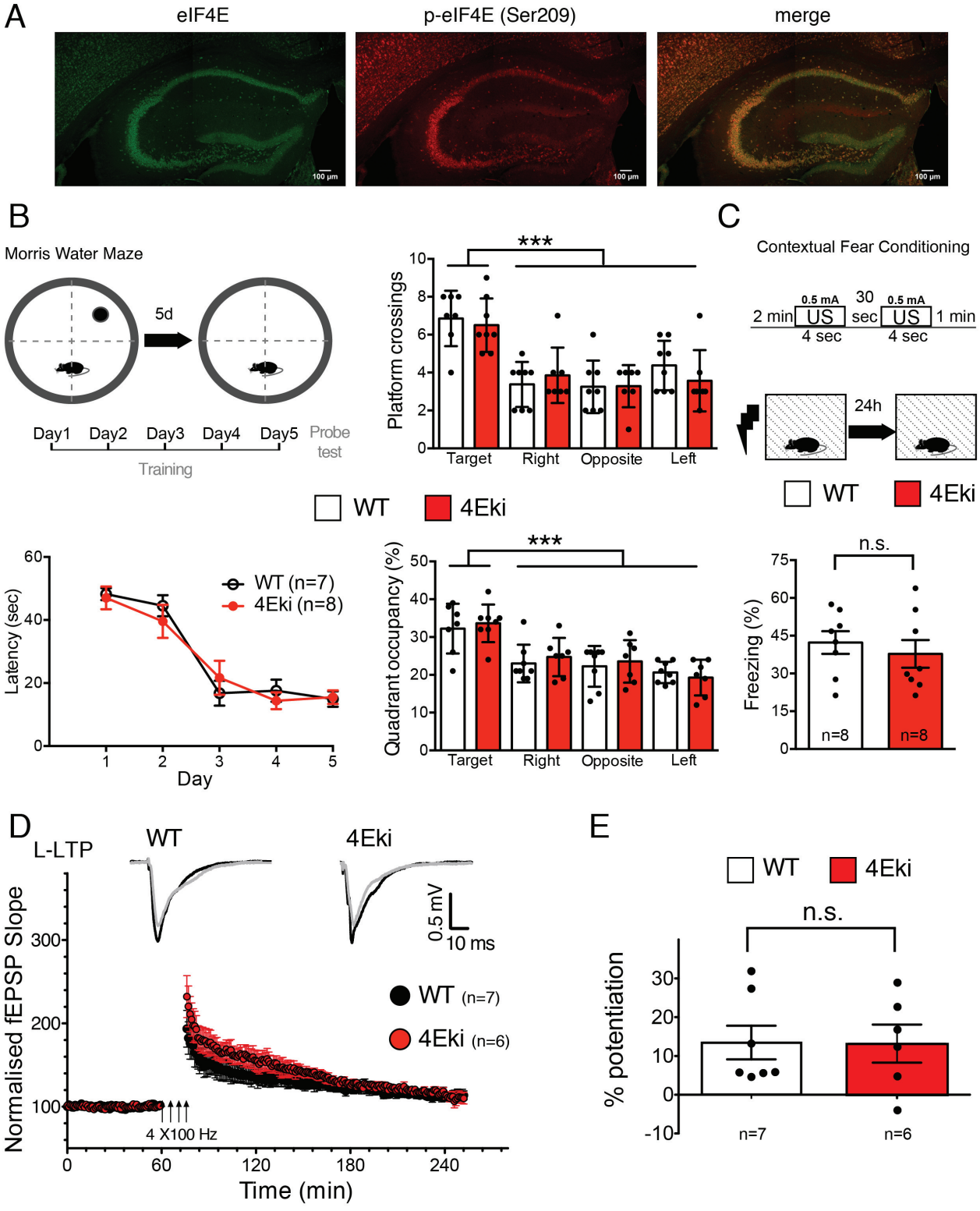

Figure 1

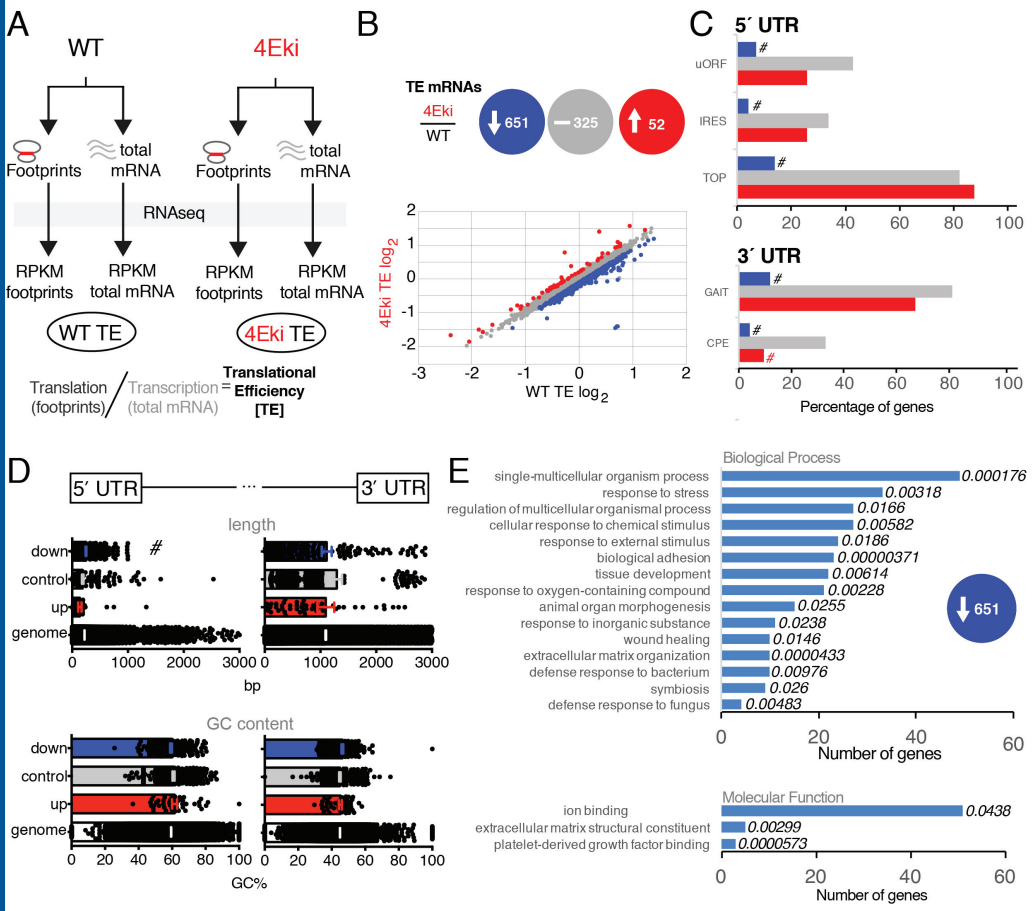

G

Pituitary hormones genes

		p value	FDR
Prl	prolactin	5.76E-21	4.44E-18
Gh	growth hormone	6.91E-07	0.000107
Pomc	pro-opiomelanocortin-alpha	0.000687	0.037809

651

ECM genes

		p value	FDR
Prg2	proteoglycan 2	0.000181	0.013937
Tnc	tenascin C	0.002159	0.075079
Mmp9	matrix metallopeptidase 9	0.002629	0.084004
Adamts16	a disintegrin-like and metallopeptidase	0.004271	0.106215
Fndc1	fibronectin type III domain containing	0.006202	0.123135
Adamts15	a disintegrin-like and metallopeptidase	0.006548	0.123135
Frem2	Fras1 related extracellular matrix protein 2	0.006998	0.123135
Tgfbi	transforming growth factor, beta induced	0.007691	0.134773
Fn1	fibronectin 1	0.008659	0.135681
Acan	aggrecan	0.008881	0.138828

Serotonin pathway **Ribosomal proteins**

		p-value	FDR
Slc6a4	serotonin transporter	5.68E-07	0.00011
Rps13	ribosomal protein S13	4.26E-08	1.64E-05
Tph2	tryptophan hydroxylase 2	4.56E-05	0.00439
Rpl35	ribosomal protein L35	1.36E-07	3.50E-05
Rpl19	ribosomal protein L19	0.03269	0.24705
Rpl10a	ribosomal protein L10A	0.03388	0.30094
Rpl37a	ribosomal protein L37a	0.02322	0.21008

Figure 2

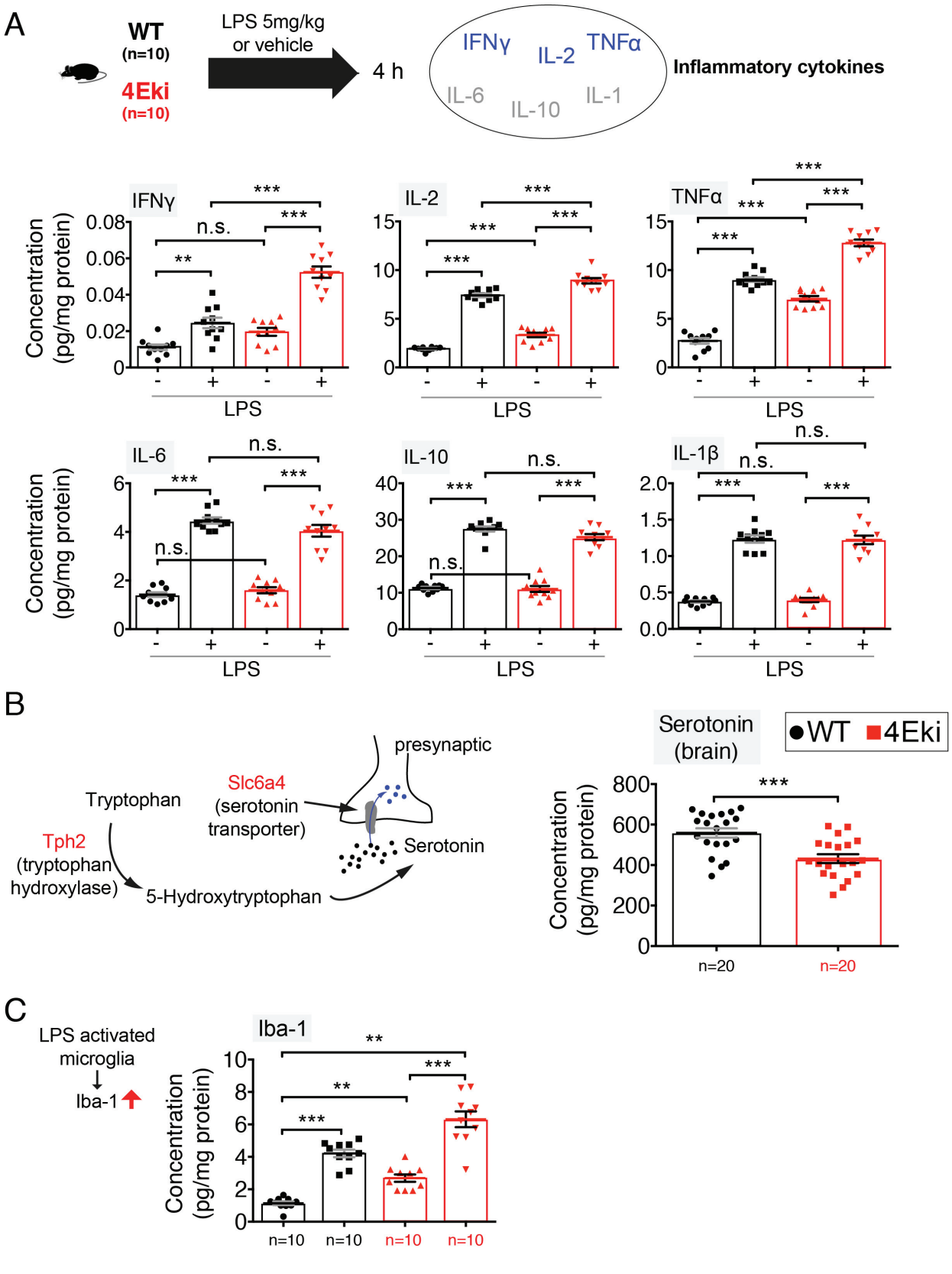

Figure 3

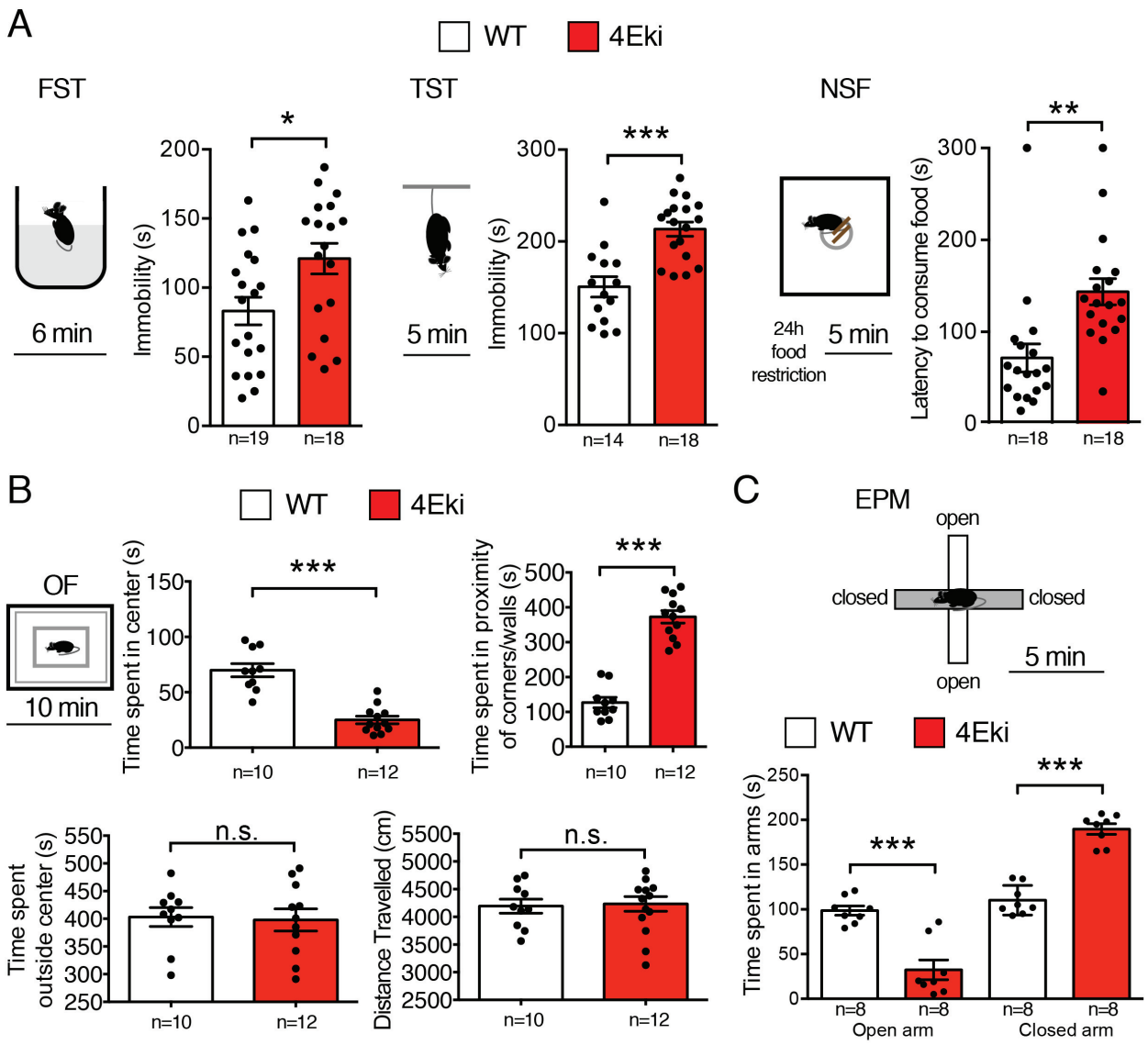

Figure 4

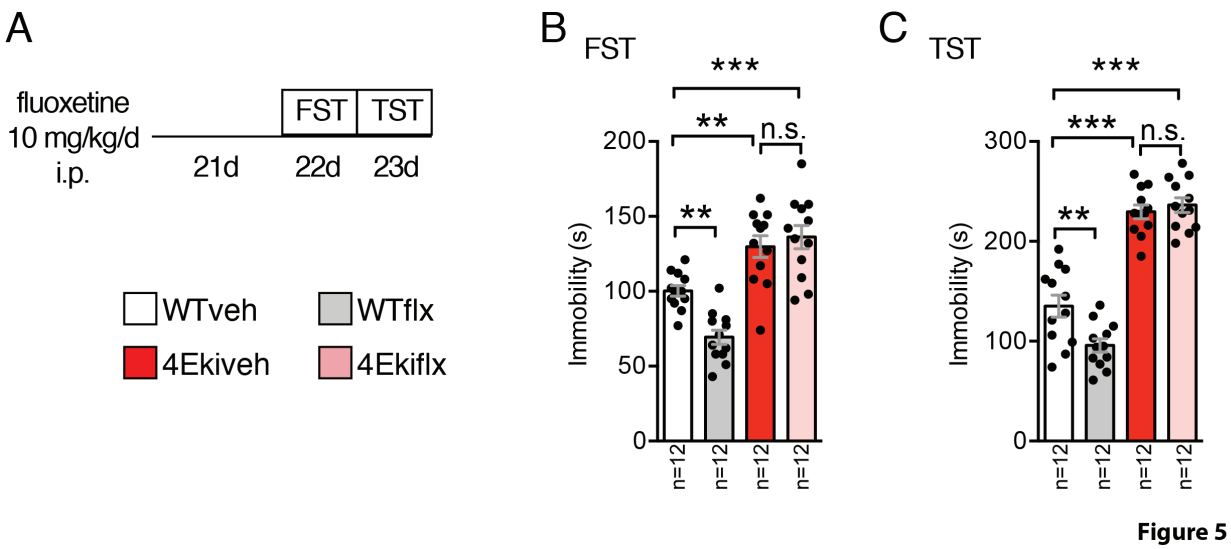

Figure 5

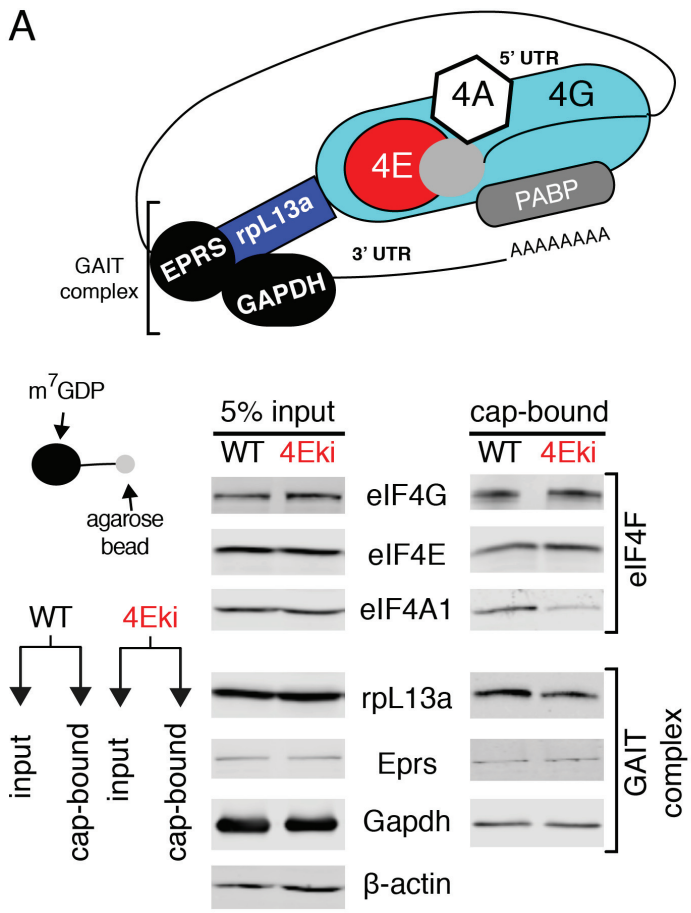

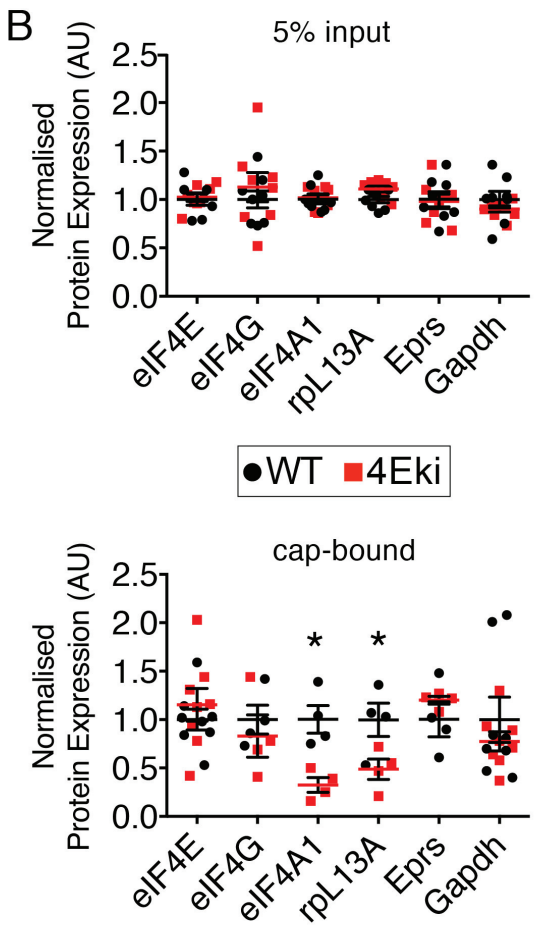

Figure 6

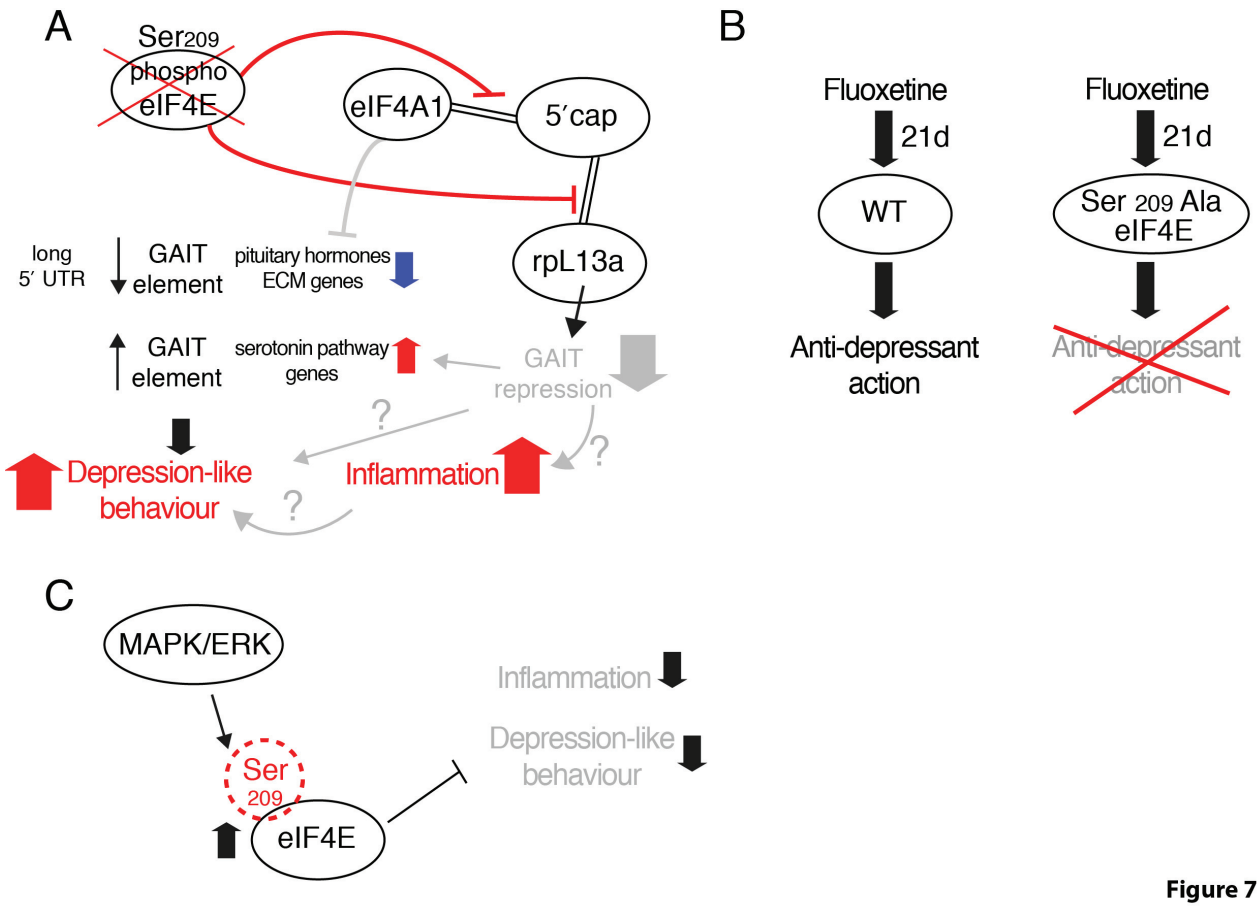

Figure 7

Protein	Host species	Supplier	Cat No	predicted kDa	WB or IF
β-actin	mouse	Sigma	A5316	42	1:5000 WB
eIF4A1	rabbit	abcam	ab31217	48	1:1000 WB
eIF4E	mouse	Santa Cruz	sc-271480	29	1:1000 WB, 1:500 IF
eIF4E phospho Ser209	rabbit	abcam	ab76256	25	1:500 IF
eIF4G1	rabbit	Cell Signaling	2498	220	1:1000 WB
RPL13A	rabbit	Cell Signaling	2765	23	1:500 WB
EPRS	rabbit	Abcam	ab31531	163	1:1000 WB
GAPDH	rabbit	Cell Signaling	2118	37	1:1000 WB

Table 2 Statistical Analysis

Test	Mean and S.E.M.	Significance and multiple comparisons	Parameter	N	Descriptive Statistics	Figure
Repeated measures ANOVA, with Tukey's post-hoc	WT: 28.404 ± 1.700 4Eki: 27.630 ± 1.792	Day: $p < 0.001$ Genotype: p= 0.758 Day x Genotype: p = 0.668	Latency (s)	WT(7), 4Eki(8)	Day: F(4,68) = 39.900 Genotype: F(1,17) = 0.098 Day x Genotype: F(4,68) = 0.595	**Fig. 1B**
	Target Quadrant: WT: 6.857 ± 0.519 4Eki: 6.500 ± 0.486 Right Quadrant: WT: 3.857 ± 0.519 4Eki 3.375 ± 0.486 Opposite Quadrant: WT: 3.286 ± 0.519 4Eki: 3.250 ± 0.486 Left Quadrant: WT: 3.571 ± 0.519 4Eki: 4.375 ± 0.486	Quadrant: $p < 0.001$ Genotype: p = 0.960 Quadrant x Genotype: p = 0.578	Number of Platform Crossings		Day: F(4,68) = 39.900 Genotype: F(1,17) = 0.098 Day x Genotype: F(4,68) = 0.595	
	Target Quadrant: WT: 32.286 ± 1.922 4Eki: 33.625 ± 1.798	Quadrant: **p<0.001** Genotype: p = 0.946 Quadrant x Genotype: p = 0.756	Quadrant Occupancy (%)		Quadrant: F(3,52) = 18.160 Genotype: F(1,52) =	

	Right Quadrant: WT: 24.714 ± 1.922 4Eki: 23.00 ± 1.798 Opposite Quadrant: WT: 23.571 ± 1.922 4Eki: 22.250 ± 1.798 Left Quadrant: WT: 19.286 ± 1.922 4Eki: 20.625 ± 1.798				0.005 Quadrant x Genotype: F(3, 52) = 0.396	
Student's *t*-test	WT: 30.75 ± 6.35 4Eki: 3.57 ± 7.02	p = 0.077	Freezing (%)	WT(8), 4Eki(8)	Genotype: F(1,19) = 0.088	**Fig. 1C**
Student's *t*-test	WT: 13.44 ± 4.337 4Eki: 13.18 ± 4.911	p=0.968	% potentiation	WT(7), 4Eki(6)	t=3.551; df=13	**Fig. 1E**
One-way ANOVA with Tukey's post-hoc	down: 247.0 ± 6.660 up: 138.0 ± 29.790 control: 188.0 ± 14.530 whole genome: 219.7 ± 1.008	up vs. down: **p=0.005** control vs. down: **p<0.001** whole genome vs. down: p=0.014 control vs. up: p=0.468 whole genome vs. up: p=0.0524 whole genome vs. control: p=0.0645	5´ UTR length	down (651), up (52), control (325), whole genome (52,678)	F (3, 53702) = 7.255	**Fig. 2D**
	down: 59.38 ± 0.555 up: 61.46 ± 1.492 control: 60.85 ± 0.602 whole genome: 59.43 ± 0.052	up vs. down: p= 0.663 control vs. down: p=0.453 whole genome vs. down: p>0.999 control vs. up: p=0.986 whole genome vs. up: p=0.611 whole genome vs. control: p=0.141	5´ UTR GC % content		F (3, 53310) = 2.018	

	down: 1112 ± 89.52 up: 1095 ± 150.6 control: 1293 ± 91.93 whole genome: 1095 ± 6.326	up vs. down: p=0.998 control vs. down: p=0.452 whole genome vs. down: p=0.998 control vs. up: p=0.780 whole genome vs. up: p>0.999 whole genome vs. control: p=0.055	3´ UTR length		F (3, 49949) = 2.146	
	down: 46.34 ± 0.534 up: 45.07 ± 0.877 control: 44.86 ± 0.458 whole genome: 44.91 ± 0.039	up vs. down: p= 0.7808 control vs. down: p=0.214 whole genome vs. down: p=0.073 control vs. up: p=0.998 whole genome vs. up: p=0.999 whole genome vs. control: p=0.999	3´ UTR GC % content		F (3, 49949) = 1.963	
One-way ANOVA with Bonferonni's post-hoc	WTveh-IFNγ: 0.011 ± 0.001 WTlps-IFNγ: 0.024 ± 0.002 4Ekiveh-IFNγ: 0.019 ± 0.002 4Ekilps-IFNγ: 0.052 ± 0.003	WTveh-IFNγ vs. WTlps-IFNγ: **p=0.003** WTveh-IFNγ vs. 4Ekiveh-IFNγ: p=0.122 WTveh-IFNγ vs. 4Ekilps-IFNγ: **p<0.001** WTlps-IFNγ vs. 4Ekiveh-IFNγ: pP>0.999 WTlps-IFNγ vs. 4Ekilps-IFNγ: **p<0.001** 4Ekiveh-IFNγ vs. 4Ekilps-IFNγ: **p<0.001**	Concentration (pg/mg protein)	WT(10), 4Eki(10)	F (3, 36) = 52.02	**Fig. 3A**
	WTveh-IL-2: 1.927 ± 0.064 WTlps-IL-2: 7.412 ± 0.177 4Ekiveh-IL-2: 3.344 ± 0.230 4Ekilps-IL-2: 8.908 ± 0.273	WTveh-IL-2 vs. WTlps-IL-2: **p<0.001** WTveh-IL-2 vs. 4Ekiveh-IL-2: **p<0.001** WTveh-IL-2 vs. 4Ekilps-IL-2: **p<0.001** WTlps-IL-2 vs. 4Ekiveh-IL-2: **p<0.001** WTlps-IL-2 vs. 4Ekilps-IL-2: **p<0.001** 4Ekiveh-IL-2 vs. 4Ekilps-IL-2: **p<0.001**			F (3, 36) = 266.7	
	WTveh-TNFα: 2.728 ± 0.289 WTlps-TNFα: 9.028 ± 0.240 4Ekiveh-TNFα: 7.062 ± 0.283 4Ekilps-TNFα: 12.80 ± 0.339	WTveh-TNFα vs. WTlps-TNFα: **p<0.001** WTveh-TNFα vs. 4Ekiveh-TNFα: **p<0.001** WTveh-TNFα vs. 4Ekilps-TNFα: **p<0.001** WTlps-TNFα vs. 4Ekiveh-TNFα: **p<0.001** WTlps-TNFα vs. 4Ekilps-TNFα: **p<0.001**			F (3, 36) = 208.7	

		4Ekiveh-TNFα vs. 4Ekilps-TNFα: **p<0.001**				
	WTveh-IL-6: 1.422 ± 0.096 WTlps-IL-6: 4.467 ± 0.128 4Ekiveh-IL-6: 1.602 ± 0.126 4Ekilps-IL-6: 4.049 ± 0.240	WTveh-IL-6 vs. WTlps-IL-6: **p<0.001** WTveh-IL-6 vs. 4Ekiveh-IL-6: p>0.999 WTveh-IL-6 vs. 4Ekilps-IL-6: **p<0.001** WTlps-IL-6 vs. 4Ekiveh-IL-6: **p<0.001** WTlps-IL-6 vs. 4Ekilps-IL-6: p=0.414 4Ekiveh-IL-6 vs. 4Ekilps-IL-6: **p<0.001**			F (3, 36) = 102.5	
	WTveh-IL-1β: 11.32 ± 0.290 WTlps-IL-1β: 27.47: 27.47 ± 0.687 4Ekiveh-IL-1β: 11.03 ± 0.830 4Ekilps-IL-1β: 25.24 ± 1.007	WTveh-IL-1β vs. WTlps-IL-1β: **p<0.001** WTveh-IL-1β vs. 4Ekiveh-IL-1β: p>0.999 WTveh-IL-1β vs. 4Ekilps-IL-1β: **p<0.001** WTlps-IL-1β vs. 4Ekiveh-IL-1β: **p<0.001** WTlps-IL-1β vs. 4Ekilps-IL-1β: p=0.176 4Ekiveh-IL-1β vs. 4Ekilps-IL-1β: **p<0.001**			F (3, 36) = 132.1	
	WTveh-IL-10: 0.376 ± 0.016 WTlps-IL-10: 1.234 ± 0.050 4Ekiveh-IL-10: 0.397 ± 0.028 4Ekilps-IL-10: 1.222 ± 0.057	WTveh-IL-10 vs. WTlps-IL-10: **p<0.001** WTveh-IL-10 vs. 4Ekiveh-IL-10: p>0.999 WTveh-IL-10 vs. 4Ekilps-IL-10: **p<0.001** WTlps-IL-10 vs. 4Ekiveh-IL-10: **p<0.001** WTlps-IL-10 vs. 4Ekilps-IL-10: p=0.414 4Ekiveh-IL-10 vs. 4Ekilps-IL-10: **p<0.001**			F (3, 36) = 135.9	
Student's *t*-test	WT-serotonin: 558.9 ± 22.96 4Eki-serotonin: 431.9 ± 21.64	**p<0.001**	Concentration (pg/mg protein)	WT(20), 4Eki(20)	t=4.025; df=38	**Fig. 3B**

One-way ANOVA with Bonferonni's post-hoc	Iba-1: WTveh: 1.141 ± 0.1125, WTlps: 4.214 ± 0.2336, 4Ekiveh: 2.686 ± 0.2241, 4Ekilps: 6.315 ± 0.4868	WTveh vs. WTlps: **p<0.001** WTveh vs. 4Ekiveh: **p=0.0047** WTveh vs. 4Ekilps: **p<0.001** WTlps vs. 4Ekiveh: **p=0.0053** WTlps vs. 4Ekilps: **p<0.001** 4Ekiveh vs. 4Ekilps: **p<0.001**	Concentration (pg/mg protein)	WT(10), 4Eki(10)	F (3, 36) = 55.02	**Fig. 3C**
Student's *t*-test	WT: 83.05 ± 10.00 4Eki: 121.06 ± 11.10	**p=0.015**	Immobility (s) FST	WT(19), 4Eki(18)	t=2.548; df=35	**Fig. 4A**
	WT: 150.50 ± 9.91 4Eki: 213.39 ± 8.74	**p<0.001**	Immobility (s) TST	WT(14), 4Eki(18)	t=4.761; df=30	
	WT: 71.67 ± 15.24 4Eki: 143.6 ± 14.23	**p=0.0015**	Latency to consume food (s) NSF	WT(18), 4Eki(18)	t=3.447 df=34	
Student's *t*-test	WT center: 69.90 ± 5.923 4Eki center: 25.00 ± 3.492 WTwall/corner: 126.9 ± 14.93 4Eki wall/corner: 372.7 ± 17.80	**p<0.001, p<0.001**	Time spent in center (s), Time spent in proximity of walls or corners (s)	WT(10), 4Eki(12)	t=6.792; df=20, t=10.32 df=20	**Fig. 4B**
	WT: 403.2 ± 17.04 4Eki: 396.8 ± 18.27	p=0.801	Time spent outside center (s)		t=0.199; df=20	
	WT: 4193 ± 125.8 4Eki: 4233 ± 133.3	p=0.830	Distance travelled (cm)		t=0.216; df=20	

One-way ANOVA with Bonferonni's post-hoc	WT: open 98.63 ± 5.227, closed 110.3 ± 5.876 4Eki: open 32.38 ± 10.97, closed 189.8 ± 5.786	**p<0.001**	Time spent in arms (s)	WT(8), 4Eki(8)	F (3, 28) = 76.91	**Fig. 4C**
One-way ANOVA with Bonferonni's post-hoc	WT veh: 100.3 ± 3.546 WT fl: 69.33 ± 4.761 4Eki veh: 129.8 ± 7.229 4Eki fl: 136.2 ± 7.817	WT veh vs. WT fl: **p=0.005** WT veh vs. 4Eki veh: **p=0.0079** WT veh vs. 4Eki fl: **p<0.001** WT fl vs. 4Eki veh: **p<0.001** WT fl vs. 4Eki fl: **p<0.001** 4Eki veh vs. 4Eki fl: p>0.999	Immobility (s) FST	WT(12), 4Eki(12)	F (3, 44) = 25.320	**Fig. 5B**
	WT veh: 135.1 ± 11.06 WT fl: 97.75 ± 6.516 4Eki veh: 229.5 ± 6.763 4Eki fl: 236.3 ± 7.334	WT veh vs. WTfl: **p=0.0081** WT veh vs. 4Eki veh: **p<0.001** WT veh vs. 4Eki fl: **p<0.001** WT fl vs. 4Eki veh: **p<0.001** WT fl vs. 4Eki fl: **p<0.001** 4Eki veh vs. 4Eki fl: **p<0.001**	Immobility (s) TST		F (3, 44) = 73.621	**Fig. 5C**
Student's *t*-test	input: WT:1.090 ± 0.05874, 4Eki: 1.048 ± 0.05977, cap: WT: 0.9975 ± 0.1723, 4EKI: 0.4875 ± 0.1062	input: p=0.630, cap: **p=0.045**	rpL13a	WT(4), 4Eki(4) or WT(8), 4EKi (8)	input: t=0.507, cap: t=2.520; df=6	**Fig. 6**
	input: WT:1.248 ± 0.335, 4Eki: 1.440 ± 0.583, cap: WT: 1.003 ± 0.142, 4Eki: 0.325 ± 0.075	input: p=0.784, cap: **p=0.005**	eIF4A1		input: t= 0.285, cap: t=4.196 df=6	
	1.088 ± 0.08499, 0.9525 ± 0.05977, cap: WT: 0.997 ± 0.222, 4Eki: 0.9175 ± 0.199	input: p=0.241, cap: p=0.798	eIF4E		input: t=1.299, cap: t=0.267, df=6	
	input: WT:1.145 ± 0.078, 4Eki: 0.905 ± 0.099 cap: WT: 1.002 ± 0.149, 4Eki: 0.830 ± 0.218	input: p=0.106, cap: p=0.544	eIF4G		input: t=1.894, cap t=0.642 df=6	
	input: WT:1.025 ± 0.108, 4Eki: 0.98 ± 0.108 cap: WT: 1.002 ± 0.185, 4Eki:0.1.2 ± 0.185	input: p=0.839, cap: p=0.382	Eprs		input: t=0.206, cap t=1.063 df=14	

	input: WT: 0.998 ± 0.091, 4Eki: 0.901 ± 0.091 cap: WT: 0.998 ± 0.254 , 4Eki: 0//775 ± 0.254	input: p=0.106, cap: p=0.544	Gapdh		input: t=1.060, cap t=0.880 df=14	